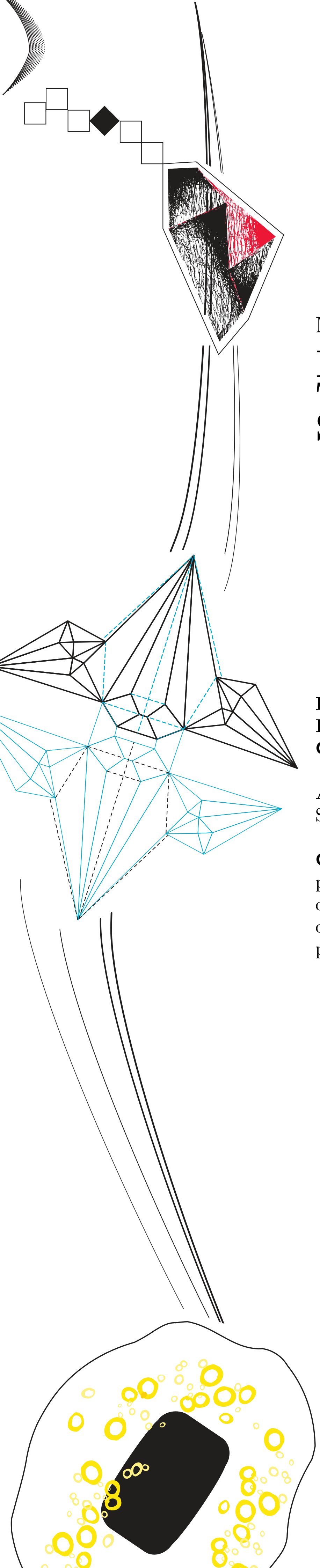

September 5, 2019

MASTER THESIS

MACROSCOPIC SINGLE CONTACT PROPERTIES OF COHESIVE SILANIZED GLASS BEADS

FACULTY OF ENGINEERING TECHNOLOGY (ET)
Department of Thermal and Fluid Engineering (TFE)
Chair of Multiscale Mechanics (MSM)

Author:
S.IJ.van der Werf

Committee:
prof.dr. A.R.Thornton
dr. T.Weinhart
dr.ir. W.K.den Otter
prof.dr.ir. C.H.Venner

msm UNIVERSITY OF TWENTE.

Preface

Nine months ago, I started this research to investigate the mixing behaviour of controllable cohesive granular material in a rotating drum. This is a large project, where several steps are involved. First, beads need to be made controllable cohesive. Second, the degree of cohesion needs to be determined. Third, the results need to be used to set the particle sizes with use of the bond number. Fourth, simulations and experiments with cohesive glass beads need to be carried out in a mixer. All these parts have interesting components for me: namely, chemistry, solid–solid interaction and fluid mechanics. Chemistry is involved by making the grains controllably adhesive. The solid–solid interaction determines the flowing behaviour of the grains, which needs to be understood before the simulations and experiments can be predicted. Finally, fluid mechanics is used to determine the flowing behaviour inside the drum.

A goal without a plan is just a wish. There was an ambitious plan, where no mistakes were allowed. Since research has an undetermined result, the final goal is not reached but still a dream. This changed the research question to investigate the macroscopic single-contact properties of cohesive silanized glass beads. I would like to thank prof.dr. A.R. Thornton for his huge enthusiasm to keep me motivated and for giving me a clear view why this result is so relevant for the community. And of course, I would like to thank dr. T. Weinhart for supervising the project, giving me detailed explanations and asked challenging questions to make this research better. Furthermore, I would like to thank the exam committee members, dr.ir. W.K. den Otter and prof.dr.ir. C.H. Venner, for taking the time and effort to review the work I did. Moving away form the subject matter, I would thank my family, who always supports me, and my girlfriend for being always there for me.

Besides the previous mentioned people, I want to thank the following people for helping me during the master project:

Name	Department	Contribution
R.J.M.Egberink*	Molecular Nanofabrication	Advising and doing the chemical treating of the glass with a silane.
L.Ricciardi	Molecular Nanofabrication	Giving instructions and helping me to measure the FTIR spectroscopy.
E.G.de Vries	Surface Technology and Trilogy	Fixing and letting me use the nanoindenter to measure the forces–displacement response of a single contact.
N.G.J.Helthuis*	Production Technology	Making the nice SEM images of the treated and untreated glass.
S.J.A.de Beer and M.Cirelli	Material Science and Technology of polymers	Discussing the chemistry of silanization.
M.Beerstra*	Student of S.J.A. de beer	Performing the AFM measurements
S.Luding	Multi Scale Mechanics	Thinking through with me the results of the force–displacement responses.

**People making a (huge) contribution to the results of this thesis.*

Enschede, September 2019,
Sven van der Werf

Abstract

The flowing behaviour of granular materials is determined by the contacts between individual solid grains. This contact behaviour is highly dependent on the particle properties; in particular we are interested in the effect of cohesion. This research experimentally investigates the contact of a single pair of macroscopic cohesive glass beads. The surface of the glass beads were functionalised via chemical silanization, attaching a silane group to the particle surface by a covalent bond to modify the cohesion.

Ideally, a monolayer around the bead should be observed that increases the dry adhesivity of the surface. However, findings indicate the silanization procedure to be moisture sensitive, especial when a trichlorosilane is used. Agglomerates of polymerized silanes are unequally divided over the surfaces, as shown on AFM measurements and SEM images.

To measure the adhesion, a CMS Nano-Tribometer was used. With this device the contact force and displacement of the particle can be measured, from which the adhesivity can be extracted. The force–displacement curves of unmodified glass were compared with the Hertzian contact model and showed a good agreement. For polymerised particles, a broad variance is noticed in the results, which we attribute to agglomeration of polymerised silanes on the surface. Some of the force-displacement curves show highly irregular behaviour. A possible explanation is that the contact occurred on a high polymerized spot, resulting in a force-displacement graph which is comparable to the ’stiff particle with soft contacts’ model of Tomas [1] for highly adhesive surfaces. In most cases, however, a contact behaviour of the functionalised particles was observed in which the loading stiffness is slightly smaller than the Hertzian behaviour of untreated glass. When unloading, the displacement increases while the normal force decreases to a point where there is still a positive normal force, thereafter, to return almost back to the previous loading curve, in such a way that the adhesion is not depended on the applied load, see Figure 1. The point where this phenomenon occurs is dependent on the load and the location of contact but does not seem to depend on velocity. The gradual change observed during cyclic loading and unloading is attributed to wear of the silane layer. An explanation why the displacement increases when the normal forces decreases, is still a matter to be researched.

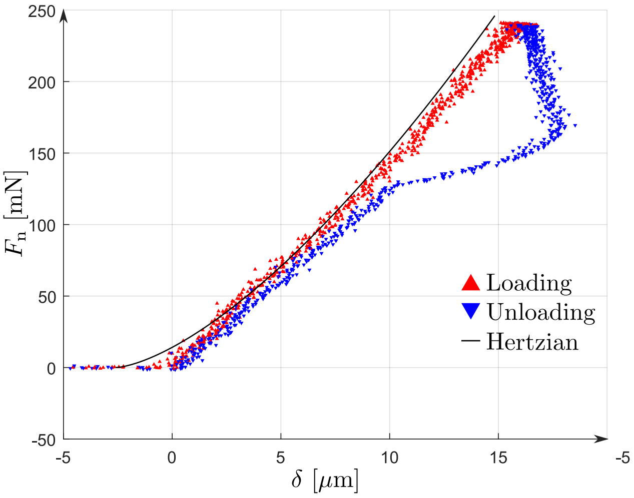

Figure 1: Force–displacement response treated bead.

Nomenclature

α	Absorption	%
$\bar{\delta}$	Dimensionless displacement	-
$\bar{F_{\mathrm{N}}}$	Dimensionless normal force	-
$\bar{P}$	Load parameter	-
$\bar{R}$	Effective particle radius	m
$\bar{v}$	Wavenumber	cm^{-1}
β	Asperity radius	m
δ	Displacement in normal direction	m
δ_{piezo}	Displacement at piezo	m
δ_{spring}	Displacement at spring	m
η	Surface density of asperities	-
γ	Surface energy	Jm^{-2}
γ_{D}	Dispersion surface energy	Jm^{-2}
γ_{L}	Surface energy of liquid	Jm^{-2}
γ_{P}	Polar surface energy	Jm^{-2}
γ_{ss}	Surface energy of both surfaces	Jm^{-2}
$\gamma_{\mathrm{ss}}^{\mathrm{DMT}}$	Surface energy according DMT	Jm^{-2}
$\gamma_{\mathrm{ss}}^{\mathrm{JKR}}$	Surface energy according JKR	Jm^{-2}
$\hat{s}$	Size ratio R_1/R_2	-
λ	Elastic parameter	-
μ	Tabor parameter	-
ν	Poisson ratio	-
ω	Rotational speed	rads^{-1}
ϕ	Gaussian distribution	-
ρ	Density	kgm^{-3}
σ	Standard deviation	-
θ	Contact angle	°
θ_{a}	Contact angle advancing	°
θ_{t}	Contact angle receding	°
ζ	Angle of response	°
ζ_{crit}	Critical angle of response	°
A	Expected area of contact	m^2
a	Radius of contact	m
Bo_{g}	Bond number for granular material	-
C	Particle - particle pair interaction coefficient	-
C_{H}	Hamaker constant	-
d	Distance between the smooth plane and reference plane	m
E	Modulus of elasticity	Pa
E^*	Effective modulus of elasticity	Pa
$F_{\mathrm{ad}}^{\mathrm{DMT}}$	Adhesion force DMT theory	N
$F_{\mathrm{n}}^{\mathrm{DMT}}$	Normal force DMT theory	N
$F_{\mathrm{n}}^{\mathrm{H}}$	Normal force Hertz theory	N
$F_{\mathrm{ad}}^{\mathrm{JKR}}$	Adhesion force JKR theory	N
$F_{\mathrm{n}}^{\mathrm{JKR}}$	Normal force JKR theory	N
$F_{\mathrm{ad}}^{\mathrm{ma}}$	Median adhesion force	N
F_{ad}	Adhesion force	N

F_{cp}	Capillary forces	N
F_{c}	Centrifugal force	N
F_{g}	Gravitational force	N
F_{H0}	Jump-in force	N
F_{n}	Normal force	N
$F_{\mathrm{n}}^{\mathrm{GT}}$	Threshold force Greenwood Tripp	N
$F_{\mathrm{n}}^{\mathrm{GW}}$	Expected normal force GW theory	N
F_{peel}	Peeling force	N
F_{vdW}	Van der Waals force	N
Fr	Froude number	-
g	Gravitational constant	$\mathrm{ms^{-2}}$
k	Spring stiffness	$\mathrm{Nm^{-1}}$
m_{p}	Mass of the particle	kg
N	Number of asperity	-
n	Expect number of contacts	-
P	Parameter	N
P_{a}	Total force between two spheres	N
R	Universal gas constant	$\mathrm{Jmol^{-1}K^{-1}}$
R_1	Radius of body 1	m
R_2	Radius of body 2	m
R_{drum}	Radius of the drum mixer	m
r_{k}	Kelvin's radius	m
R_{p}	Particle radius	m
s	Separation between atomic planes	m
s_0	Characteristic adhesion distance	m
T	Temperature	K
t	Time	s
t_{av}	Average time	s
V_{mol}	Molar volume	$\mathrm{m^3mol^{-1}}$
w	Work done by adhesion	$\mathrm{Jm^{-2}}$
z	Height of asperity	m
MAD	Median absolute deviation	N
RH	Relative humidity	%
$\mathrm{RH_{av}}$	Average relative humidity	%
RMS_f	Flattended roughness of the curved surface	m

Contents

1 Introduction

Sugar in a bowl, screes at the bottom of a mountain, peas and gravels are all examples of granular materials. These materials are a conglomeration of macroscopic discrete solid particles in a fluid such that each piece interacts with its nearest neighbours [2]. This gives them the unique ability to behave as a solid, liquid or gas without a change in temperature. All these forms come together in an hourglass. At the top, the grains are almost at rest, such that they behave as a solid. When the sand is falling through the small gap, it behaves as a gas, and liquid-like when the sand is flowing as an avalanche before it comes to rest.

Granular material are processed in a plethora of applications, such as cosmetics, pharmacy, and the food industry. Understanding their behaviour is important to making effective machines. This is a challenging topic, as the contacts between the individual particles determine the behaviour of the complete bulk. It is particularly challenging when the grains have different properties from each other, which is the case in many applications. The species may differ in size, shape, density, adhesion, and so on. When grains with different properties behave as a liquid or a gas, segregation may occur. Particle–size difference is the most dominant segregation mechanism [3]. Small particles can move through the voids of the larger species, resulting in large particles floating on the smaller grains as they flow (granular flow). This phenomenon is shown in Figure 1.1. Theoretical models have been investigated to predict the particle-size segregation [4, 5, 6]. Here, only the size and density of the grains are changed.

Several other mechanisms contribute to the total force at the point of contact, including elastic and plastic deformation, friction at the particle surface, and cohesion. In this work, we focus our attention on the latter, since many grains are adhesive, especially for fine powders, and when grains are sticky, it affects the mixing behaviour significantly [7]. There is a distinction between 'dry' and 'wet' cohesion: wet adhesion is caused by liquid bridges [8] and dry by van der Waals forces, which become dominant for very small particles [1]. Several studies have accomplished an increase the dry cohesion of glass by silanization [9, 10, 11]. However, the results are contradictory and not reproducible. Therefore, to single out the effect of cohesion on contact properties, we chemically treat glass beads with a silane in as controlled a manner as possible. We then measure the force–displacement response of the beads to see the effect of the silane on a macroscopic glass bead. Those properties can be used in simulations and to predict the mixing behaviour.

The main question in this thesis is the following:
Can chemical silanization be applied to make glass beads controllably cohesive on the macroscopic scale?

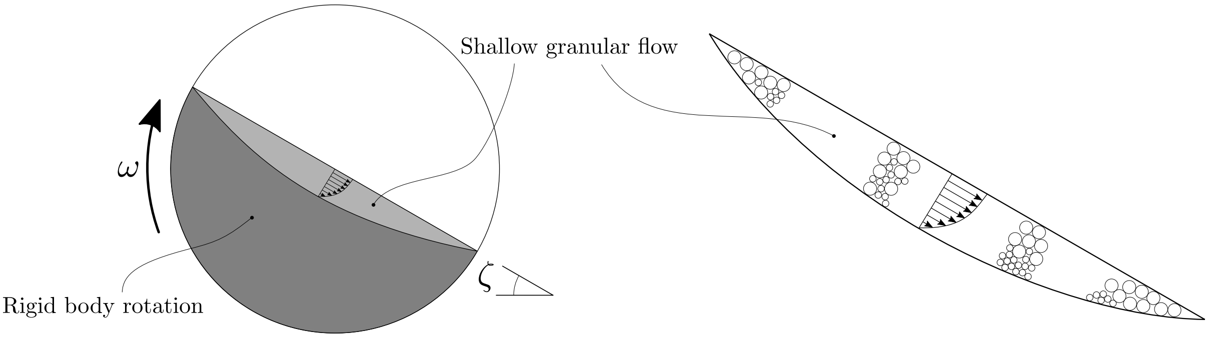

Figure 1.1: Schematic overview of flow types inside a drum mixer.

2 Theoretical background

In this chapter, we investigate the theory behind the topic to first examine which properties are important by comparing different dimensionless numbers. Second, the existing force–displacement contact models are compared to each other. Third, we investigate the adhesion force mechanisms between particles and investigate how to control the cohesion of glass beads. Finally, we explore how to determine the beads stickiness and how to move from the microscopic to the macroscopic interface.

2.1 Dimensionless numbers

In mixing segregation is determined by the particle properties. Particle–size is the most significant one [3]. Several dimensionless numbers are important, especially when cohesion plays a role. Those are explained in the following sections.

2.1.1 Froude number

The Froude number (Fr) is the ratio of the flow inertia over the external forces. With this number it is possible to determine the flow regimes inside a drum, see Figure 2.1. For a rotating drum, the external forces are due to gravity ($F_\mathrm{g} = m_\mathrm{p} g$, where m_p is the mass of the particle and g the gravitational constant) and the flow inertia due to centrifugal forces ($F_\mathrm{c} = m_\mathrm{p}\omega^2 R_\mathrm{drum}$, where R_drum is the drum radius and ω the rotational speed). The Froude number for a rotating drum is defined as

$$Fr = \frac{\text{Flow inertia}}{\text{External field}} \quad \xrightarrow{\text{Drum mixer}} \quad Fr = \frac{\omega^2 R_\mathrm{drum}}{g}. \tag{2.1}$$

There are six flow regimes classified as illustrated in Figure 2.1 [12, 13]. In the surging regime, slipping occurs. All particles move as a rigid body and when the critical angle of response (ζ_crit) is reached, the block of particles falls. In this regime, particles are not moving relative to each other. The same is true when the particles are in the centrifuging regime: all particles are fixed at the drum wall. In the slumping mode, the particles move as a rigid body until the critical angle of response is reached. An avalanche of particles falls down, and thereafter, particles behave as a rigid body again. Mixing in slumping regime is slow process. These three regimes are not relevant for the mixing industry.

In the rolling and cascading regimes, a continuous avalanche of particles takes place inside the mixer. In this free flow of particles, segregation or mixing occurs, depending on the particle properties. Cascading is the highest flow regime before the particles become airborne. Both mixing regimes are relevant for industry.

In the cataracting regime, particles are centrifuged into the air, but the external forces are still too great, such that the particles fall again. The segregation mechanism in this regime is changing from sieving to fluidisation effects [14]. This regime is relevant for industries in which grains needed to be crushed.

When the beads are cohesive to each other, the mixing behaviour changes completely. In such cases the Froude numbers in Figure 2.1 are no longer valid, and higher Froude numbers are required to transition to the next higher regime [11].

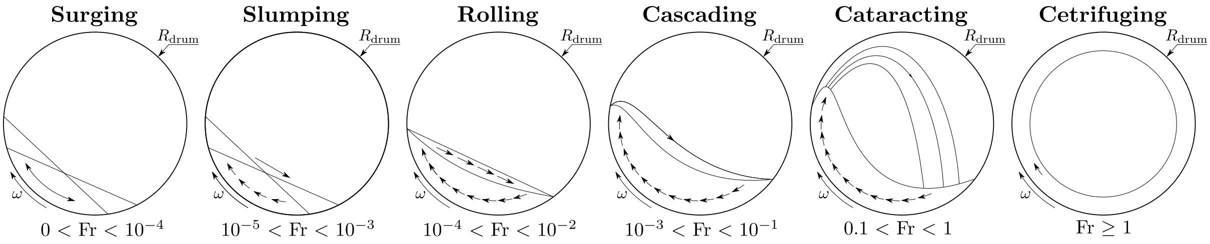

Figure 2.1: Six mixing regimes depending on the Froude number for non-cohesive grains.

2.1.2 Bond number

The Bond (Bo_{g}), or Eötvös number, is a dimensionless number defined as the ratio of the attractive force over the external field forces. With this number, it is possible to determine the rate of cohesion. For granular material driven by gravity, the Bond number is defined as [15]

$$Bo_{\text{g}} = \frac{\max(F_{\text{ad}})}{\frac{4}{3}\pi R_{\text{p}}^3 \rho g}, \tag{2.2}$$

where R_{p} is the radius of the smallest bead, ρ is the density, and F_{ad} is the force due to the attractive forces. The maximum adhesion force is used in calculating the Bond number. In polydisperse materials, the adhesion force is dependent on which bead is touched. Nase et al. derived the bond number from a monodisperse system. In a polydisperse system, the radius of the smallest bead is chosen, since the motion of less massive particles is dominated by the larger species [16].

In a bidisperse system, segregation occurs when $Bo_{\text{g}} < 1$ and mixing when $Bo_{\text{g}} > 1$ [17]. Once the beads are made cohesive, different bead sizes will be selected to change the Bond number while the size ratio ($\hat{s} = R_1/R_2$) is kept constant. The size ratio determines the rate of particle–size segregation, which is greatest when $\hat{s} \approx 2$ [6].

2.2 Contact models

Contact models are derived from the study of the deformation of solid objects that are in contact to each other. Since every individual particle interacts with its direct neighbours, it is important to use a model which best describes the response. This could be in tangential direction or in normal direction (load is applied perpendicularly to the surface). Over the years, multiple contact models for solid particles have been derived, all with different properties or assumptions. Tomas assembled an overview of these models [18]. The most common are summarised here along with some well known models for cohesive powders.

2.2.1 Hertz

Hertz derived a model to predict the elastic deformation of a point contact [19]. The model relates the circular area where a sphere contacts a plane or another sphere to the elastic deformation properties of the material. This model is derived for contacts without adhesion, all tension forces are ignored. Experimental results show good agreement with the model after a certain applied normal load is reached but the models fails for smaller initial loads. At these lower loads, the contact area is larger than suggested by Hertz and tends towards a finite value when approaching to zero loading, suggesting there is an attractive surface force between the solids which become less significant at higher loads [20]. Nevertheless the radius of contact (a) according to Hertz can be computed with the following equation

$$a = \left(\frac{3}{4}\frac{\bar{R}}{E^*}F_{\text{n}}\right)^{\frac{1}{3}}, \tag{2.3}$$

where F_n is the force applied in normal direction and E^* is the equivalent Young's modulus which can be calculated with

$$E^* = \left[\frac{1-\nu_1^2}{E_1} + \frac{1-\nu_2^2}{E_2}\right]^{-1}, \tag{2.4}$$

where ν is the Poisson ratio and E is the Young's modulus of the material. Subscripts 1 and 2 are for the bodies in contact. $\bar{R}$ is the equivalent radius, which varies for different cases:

$$\bar{R} = \left(\frac{1}{R_1} + \frac{1}{R_2}\right)^{-1} \quad \text{sphere - sphere} \tag{2.5}$$

$$\bar{R} = \left(\frac{2}{R_\mathrm{p}}\right)^{-1} \quad \text{two equal spheres} \tag{2.6}$$

$$\bar{R} = R_1 \quad \text{sphere–flat, since } R_2 \to \infty \tag{2.7}$$

Equation 2.3 can be rewritten to the normal force according to Hertz (F_n^H) as a function of the deformation in normal direction (δ), when assuming the contact radius is equivalent to $a \approx \sqrt{\bar{R}\delta}$.

$$F_\mathrm{n}^\mathrm{H}(\delta) = \frac{4}{3}E^*\sqrt{\bar{R}}\delta^{\frac{3}{2}} \tag{2.8}$$

Several assumptions are made in the Hertz model:

- The deformations are small within the elastic limit.
- The contacting area is much smaller than the dimensions of the bodies in contact, $a \approx \sqrt{\bar{R}\delta}$.
- Each body is considered as a perfectly smooth spherical elastic body.
- The surfaces are frictionless.
- There are no attractive forces between the bodies.

2.2.2 JKR Model

The contact mechanics of Hertz do not assume adhesion forces between the contacting bodies, although, in almost all cases, there are some attractive forces between two solids. These become important when the loads is reduced towards zero and can have a significant effect on the solids behaviour. Johnson, Kendall and Roberts (JKR) derived an additional model to describe the influence of adhesion [20] by balancing the stored elastic energy, the mechanical energy and the loss in surface energy.

When considering the surface energy effects the contact radius can be calculated with

$$a^3 = \frac{3}{4}\frac{\bar{R}}{E^*}\left[F_\mathrm{n} + 3\gamma_\mathrm{ss}\pi\bar{R} + \sqrt{6\gamma_\mathrm{ss}\pi\bar{R}F_\mathrm{n} + \left(3\gamma_\mathrm{ss}\pi\bar{R}\right)^2}\right], \tag{2.9}$$

where γ_ss is the surface energy per unit area (i.e., of both surfaces). From Equation 2.9, we can derive an equation to calculate the normal force according JKR ($F_\mathrm{n}^\mathrm{JKR}$) as a function of the displacement. The derivation can be found in Appendix A. The result is shown here

$$F_\mathrm{n}^\mathrm{JKR}(\delta) = \frac{4}{3}E^*\sqrt{\bar{R}}\delta^{3/2} - \sqrt{8E^*\gamma_\mathrm{ss}\pi(\bar{R}\delta)^{3/2}}. \tag{2.10}$$

Minimisation of the total force (Equation 2.10) will result in the adhesion force, according JKR ($F_\mathrm{ad}^\mathrm{JKR}$)

$$F_\mathrm{ad}^\mathrm{JKR} = -\frac{3}{2}\pi\bar{R}\gamma_\mathrm{ss}. \tag{2.11}$$

Assumptions made in the JKR model:

- The same assumptions are made as in the Hertz model, except an adhesion force is assumed.
- Elastic energy is calculated from an idealised force–displacement curve, where the surface forces are neglected.

2.2.3 DMT Model

The Derjaguin, Muller and Toporov (DMT) model is an alternative model that includes adhesion [21, 22]. The difference with JKR model is that they assuming the attractive forces are contributed to a ring outside the contacting area. The contact area is defined as

$$a^3 = \frac{3}{4}\frac{\bar{R}}{E^*}\left(F_\mathrm{n} + 2\gamma_\mathrm{ss}\pi\bar{R}\right). \tag{2.12}$$

This equation is rewritten in a form where the normal force according the DMT theory ($F_\mathrm{n}^\mathrm{DMT}$) is a function of the elastic deformation

$$F_\mathrm{n}^\mathrm{DMT}(\delta) = \frac{4}{3}E^*\sqrt{\bar{R}}\delta^{3/2} - 2\gamma_\mathrm{ss}\pi\bar{R}. \tag{2.13}$$

In the DMT model, the pull-off force in the normal direction ($F_\mathrm{ad}^\mathrm{DMT}$) is

$$F_\mathrm{ad}^\mathrm{DMT} = -2\pi\bar{R}\gamma_\mathrm{ss}. \tag{2.14}$$

Assumptions made in the DMT model:

- The same assumptions are made as in the Hertz model, except an attractive force is assumed.
- The adhesion is contributed to a ring outside the contacting area.
- The adhesion force is independent of the applied normal load.

2.2.4 Stiff particles with soft contacts

Tomas assumed a model of 'stiff particles with soft contacts' which is derived from reasonable particle and continuum mechanics [1]. See Figure 2.2 for the force–displacement diagram. The model is derived for particles which are isotropic, stiff, linear elastic, spherical and have contacts consisting of soft smooth surfaces. Cohesive glass beads have all of these properties. This could be a useful model for silanized glass beads.

Tomas noticed that in all models with adhesion a constant adhesion force added, and made the assumption that all the attractive forces are due to Van der Waals forces only. When the beads have zero overlap, the attraction is formed by the long-range adhesion force F_H0, which is called the jump-in force. When the normal load is increased the bead deforms non-linearly elastically, according to Hertz theory. At a certain point, the soft layer starts to deform plastically in a linear manner. When unloading, hysteresis is obtained, until it reaches the adhesion limit. After the adhesion limit, the contact breaks and detached with a pull-off force. The pull-off force is dependent on the applied normal load.

However, this is a quite complex model with non-linearities and discontinuities. Luding derived a similar but simple contact model which still describes the contacting behaviour well [23]. The jump-in force can be calculated with the equation of Dahneke [24]

$$F_\mathrm{H0} = \frac{C_\mathrm{H}\bar{R}}{6s_0^2}, \tag{2.15}$$

where C_H is the Hamaker constant and s_0 the characteristic adhesion distance on molecular scale ($s_0 \approx 0.3 - 0.4\mathrm{nm}$). The distance is depending on a lot of factors like roughness and absorbed liquid layers due to humidity. The Hamaker constant can be determined using the Lifshitz theory [25].

The following assumptions are made in the model:

- The contact displacement is small in comparison to the particle radius $\delta/R_\mathrm{p} \ll 1$.
- The material stiffness is high enough to neglect the volumetric changes.
- The surface stresses are low enough that the rigid particle undergoes a change in particle shape.
- All attractive forces are due to Van der Waals forces only.

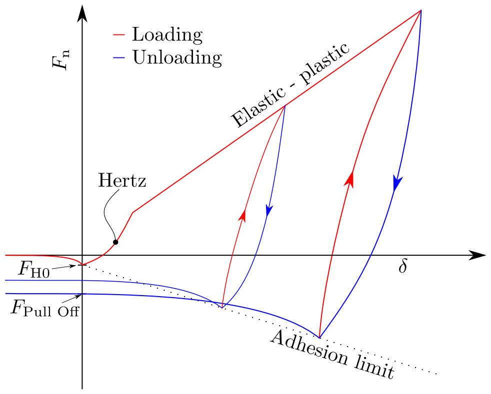

Figure 2.2: 'Stiff particles with soft contacts' contact model [1].

2.2.5 Model selection

The most common models for stiff materials or stiff materials with soft contacts are summarised above. Selecting one of the models, an adhesion map is provided [26], shown in Figure 2.3. The Bradley (Rigid) model has not yet been mentioned: the elastic deformations are small in comparison with the surface forces such that it can be assumed to be rigid. The M-D model is a transition between the DMT model and the JKR, where the separation constant is changed from 2 to 3/2 (Equations 2.14 and 2.11). This change is due to the adhesion of capillary forces. The elastic parameter (λ) is determined with the Tabor parameter (μ), which is defined as [27]

$$\mu \equiv \left(\frac{\bar{R} w^2}{E^{*2} s_0^3} \right)^{1/3}, \tag{2.16}$$

where s_0 is the equilibrium separation in the Lennard–Jones potential, and w is the Dupré work of adhesion, which is in therms of surface energy $w \equiv \gamma_1 + \gamma_2 - \gamma_{12}$, where subscripts 1 and 2 denote the surface energy of the bodies, and 12 is the interfacial energy between the two. Considering only dispersion forces, the work of adhesion can be approximated with $w \approx 2\sqrt{\gamma_1 \gamma_2}$ and for two equal surfaces $w \approx 2\gamma_1 = \gamma_{ss}$ [28].

To determine the load parameter ($\bar{P}$), we need to know parameter P, which is defined as $P = F_n^H + P_a$, where P_a is the total force between two spheres [29]:

$$P_a = \frac{8\pi w \bar{R}}{3} \left[\frac{1}{4} \left(\frac{s}{s_0} \right)^{-8} - \left(\frac{s}{s_0} \right)^{-2} \right]. \tag{2.17}$$

Here, s is the separation between the atomic planes.

The adhesion map is derived if the contacts are hard, without any plastic deformation. When the contact is soft, the 'stiff particles with soft contacts' model is a more realistic choice.

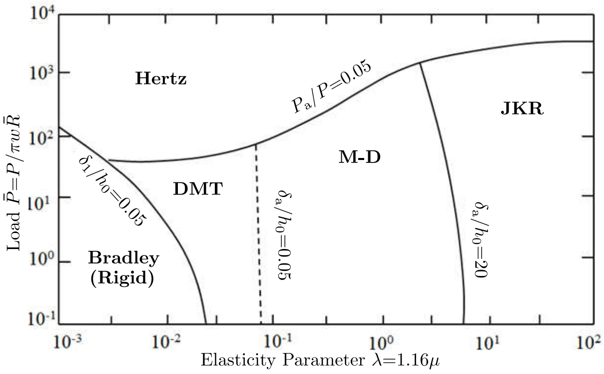

Figure 2.3: Adhesion map [26].

2.3 Adhesion force mechanics

In the contact model analysis we saw different mechanisms to predict the pull-off force due to adhesion. Bodies with their physical surfaces in contact may be attractive or repulsive to each other. These forces are generally caused by multiple kinds of surface forces, such as van der Waals (F_{vdW}), meniscus or capillary forces (F_{cp}), and other interacting surface forces, like electrostatic forces, are not considered in this work. The combined adhesion forces can be calculated with Equation 2.18.

$$F_{\mathrm{ad}} = F_{\mathrm{vdW}} + F_{\mathrm{cp}} + \cdots \tag{2.18}$$

These two forces are explained in more detail in the following sections.

However, the motion of the beads is described by Newton's second law, where the particles mass determines its movement, while the stickiness of each body is determined by the contact area (Bond number). The mass scales with the radius cubed and the area with the radius squared. If the beads decrease in size, the adhesion becomes more dominant. Richard et al. classified the grains by there size [30], and Tomas determined the degree of adhesion [31]. In Table 2.1, the quantification can be read.

Table 2.1: Subdivision of granular materials.

Description [30]	Size (R_{P})	Degree of adhesive [31]
Broken solid	>3mm	almost not
Granular solid	100μm - 3mm	almost not
Granular powder	10μm - 100μm	slightly
Super fine powder	1μm - 10μm	adhesive
Ultra fine powder	0.1μm - 1μm	very
Nano sized particles	<0.1μm	-

2.3.1 Van der Waals force

In case of fine dry particles, where relative humidity (RH) <10%, the adhesion is mainly due to the van der Waals force [32]. The van der Waal forces are forces of attraction or repulsion between atoms, molecules and surfaces. The forces are caused by correlations in fluctuating polarisations of nearby particles [25]. It is the weakest intermolecular force, but when there are multitudes of such interaction are present, it can contribute significantly. The distance between the surfaces has a strong effect on the magnitude of this force. For perfectly smooth, non-deformed, stiff particles, the sort range attractive force can be calculated with

$$F_{\mathrm{vdW}} = \frac{C_{\mathrm{H}}\bar{R}}{6s^2}. \tag{2.19}$$

The Hamaker constant for $\mathrm{SiO_2}$ particles is $C_{\mathrm{H}} = 6.6 \cdot 10^{-20}$ in a vacuum [33]. This can also be calculated

$$C_{\mathrm{H}} = \pi^2 C \rho_1 \rho_2, \tag{2.20}$$

where ρ_1 and ρ_2 are the number densities and, C is the particle-particle pair interaction coefficient. However, this is a quite complex task to get the numbers and tends to be easier to measure for macroscopic bodies, where the surface is not ideal.

2.3.2 Capillary force

Capillary forces are meniscus forces caused by surface tension of three mediums: a solid, a liquid and a gas. If the surface tension of the solid is lower than that of the liquid, the liquid climbs to the solid. When the surfaces are in contact or close to each other in humid conditions, a capillary force is present. The capillary force may be repulsive if the surface is hydrophobic or attractive if the surface is hydrophilic [34]. The force strongly depends on RH, the roughness of the contacting bodies, the radius of the sphere and the surface tension of the bodies [35].

In normally humid conditions, there are always a couple of monolayers water on the surface due to absorption. The absorption phenomenon is the accumulation of a fluid (liquid or gas) material on the surface of a solid [36]. The solid is called *absorbent*, the material attached to the surface *adsorbate* and the free material in the fluid is the *adsorpt*. Depending on the RH several monolayers will form. Asay et al. determined the evolution of water layer formation on silica oxide at room temperature [37]. The first water monolayer is formed at around 10% RH. At this stage, there is only solid–solid interaction, where only the van der Waals forces are causing adhesion. Between 10% and 30% RH, layers will form until three layers are present. The behaviour of these layers is 'ice-like': there is a layer of water that does not go move from the absorbent. Between 30% and 60% RH, a transition takes place: a layer develops which starts to move like a liquid. Above 60% RH, multiple liquid-like layers develop, such that a meniscus is formed. An increase of water layers (above 70% RH) decreases the adhesion force, since screening of van der Waals forces takes place [25]. Figure 2.4 shows the layer formation around a bead in contact with a flat substrate.

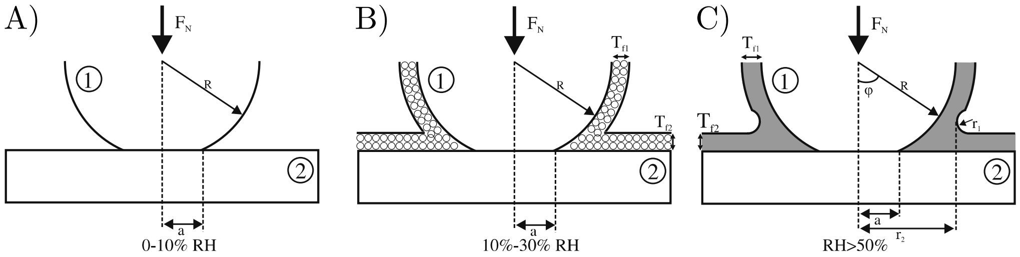

Figure 2.4: Water layer formation at the surfaces. A) There is a solid–solid contact (RH≤ 10%). B) An ice-like layer is formed (10%<RH<30%). C) An meniscus starts to develop (RH≥30%) [35].

Yaqoob et al. proposed a model in which the adhesion force is predicted based on the RH and they validated it with several tests [38]. Figure 2.5 shows the results of the measurements and their proposed model. As can be seen, the adhesion is dependent on the humidity. Yaqoob et al. based their work on a single asperity contact [35], where surface roughness was excluded as much possible. The results in Figure 2.5 represents the adhesion of relatively smooth material, such that more or less a single asperity contact is measured.

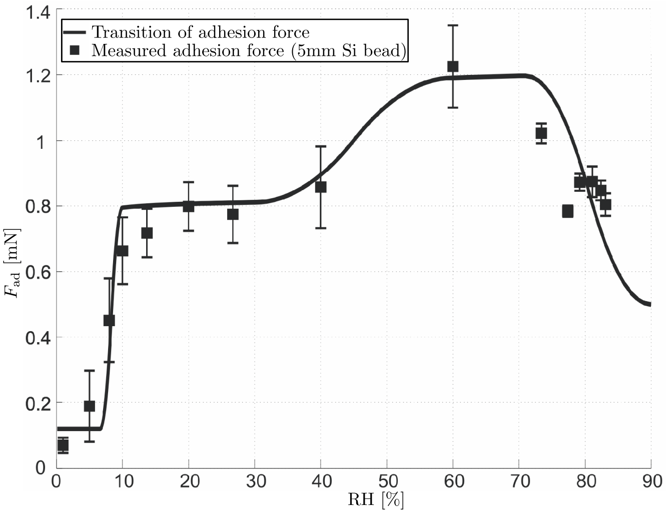

Figure 2.5: Adhesion force depending on the RH for a smooth surface [35].

When a 'rough' surface is present, multi-asperity contacts needs to be considered. This significantly changes the adhesion. All the above models assumed smooth surfaces. If the absorbate layers are liquid-like (above 50% RH), a meniscus will form in the valleys of the surface roughness before a meniscus forms between the point of contact. An increase of the roughness decreases the adhesion force, which has been shown by many researchers: for example, Liu et al. and Fuchs et al. [39, 40].

To solve the problem of whether a rough surface in humid conditions is adhesive or not due to capillary forces, we make use of the Kelvin equation. The Kelvin equation describes the change in RH to a radius of the droplet (r_k) of the liquid vapor interface. The equation is

$$r_\mathrm{k} = \frac{\gamma_\mathrm{L} V_\mathrm{mol}}{RT\ln(\mathrm{RH})}, \tag{2.21}$$

where γ_L is the liquid surface energy, V_mol the molar volume, R the universal gas constant and T the temperature. For water at 20°C, $\gamma_\mathrm{L} V_\mathrm{mol}/RT$=0.54nm [25]. When the RH decreases, r_k decreases also. McFarlane and Tabor found when the asperity size is smaller than r_k the adhesion force due to capillarity reaches a maximum [41]. This adhesion force when there is a liquid layer on the surface is

$$F_\mathrm{cp} = 2\pi\bar{R}\gamma_\mathrm{L}\left[\cos(\theta_1) + \cos(\theta_2)\right], \tag{2.22}$$

where θ_1 and θ_2 are the contact angle of the liquid and the two bodies.

This analogy is not complete. If two rough materials are in contact, the asperities can interlock with each other. In such a case, the adhesion due to capillarity is already seen before the critical RH is reached. This is not considered in previous models. However, the surface roughness together with the RH play an important role in the adhesion force between two contacting bodies. It is important to measure with a constant RH to keep the contribution of capillarity forces as constant as possible.

2.4 Surface Roughness

The surface roughness plays an important role in the contact and adhesion mechanics. All the contact models are derived for smooth surfaces. In real applications the surfaces have always a certain roughness, this has an impact on the adhesion force and the contact angle (Wenzel equation). Greenwood and Williamson pioneered in with there multiasperity contact model [42]. In this model the surface is represented as a set of independent asperities with constant radius β and the asperity height varied with the Gaussian probability

$$\phi(z) = \frac{1}{\sigma}e^{-z^2/2\sigma^2}, \tag{2.23}$$

where σ the standard deviation of the asperity peaks and z is the asperity distance, see Figure 2.6. When the distance between the smooth rigid surface and the reference plane is d, the probability of the contact for an asperity is given by

$$\mathrm{Prob}(z > d) = \int_d^\infty \phi(z)dz. \tag{2.24}$$

If there are N numbers of asperity, the expected number n of contact will be

$$n = N\int_d^\infty \phi(z)dz. \tag{2.25}$$

The expected total area of contact A is given by

$$A = \pi N\beta\int_d^\infty (z-d)\phi(z)dz. \tag{2.26}$$

The expected load (F_n^GW) will be

$$F_\mathrm{n}^\mathrm{GW} = \frac{4}{3}NE^*\beta^{1/2}\int_d^\infty (z-d)^{1/2}\phi(z)dz. \tag{2.27}$$

A lot of assumptions are made in this model. However, they are still relevant for the industry. The assumptions are: there is one smooth surface against a rough one. All the asperities have the same radius β and deforms according Hertz theory. The height of asperities vary randomly, the probability has a height between z and $z+dz$ above the reference plane. Considering a rough sphere against a rough sphere this, analogy changes.

Greenwood and Tripp considered a multi asperity flat surface in contact with a smooth spherical body [43]. They founded a threshold force (F_n^GT), during monotonic loading of a rough non conforming contact. The force is

$$F_\mathrm{n}^\mathrm{GT} \cong 100\mathrm{RMS}_f\ E^*\sqrt{2R\ \mathrm{RMS}_f}, \tag{2.28}$$

where RMS_f is the flattened roughness of the curved surface. After this threshold force, Hertz model is valid.

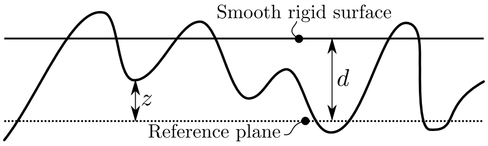

Figure 2.6: Surface roughness

2.5 Surface modification

Glass beads are used in a number of research studies. They are spherical, stiff, chemical resistant and almost non-cohesive. These properties makes them a useful material to determine mixing behaviour in general. Another useful quality is that the surface can be silanized: that is, the glass surface is covered with a monolayer of chemically reactive silane compounds. This created soft layer will increase the adhesiveness or the non-cohesion. By varying the type of silane compound, different levels of adhesion can be achieved [9, 10, 11, 44].

2.5.1 Silanization

Soda lime glass or borosilicate spheres consist of around 72% silicon dioxide and 28% other, mostly boric, oxides. On every silicon dioxide molecule it is possible to make a covalent bond with a silane couple agent. The couple agent consists of a silicon atom with a hydrolyzable group and an organofunctional group. The hydrolyzable group, typically alkoxy, acyloxy, halogen or amine, can inelaborate react with a hydrogen atom and is used to attach the agent onto the glass surface [45]. The organofunctional group, which covers the outer surface of the functionalised particle, gives the glass surface different properties depending on chemical structure. Due to the easily reacting coupling agent, this is often called a self-assembled monolayer (SAM). Figure 2.7 gives an overview of the silanization process.

The silane will react to surfaces with hydroxyl groups (OH). To achieve this, the glass beads need to be cleaned with an oxidising acid. For example, hydrogen chloride or peroxymonosulfuric acid. Peroxymonosulfuric acid is a mixture of sulfuric acid H_2SO_4 (95–97%) and hydrogen peroxide (H_2O_2) with a concentration of 50%, known as Piranha solution. Contamination is removed from the surface, and most of the organic matter is removed. To remove any acid, the beads are then cleaned several times with deionised water and dried. This process makes the surface hydrophilic [46] (Figure 2.7 middle).

After cleaning, the silanization process can be started. There are several ways in order to create a SAM [47]. The most straight forward one for small-scale experiments is to dissolve the silane in a dry solvent. Depending on the hydrolyzable group of the silane, it can be extremely sensitive to moisture. This means the solvent may not contain any liquid. McGovern et al. tested different solvents and found out the densest monolayer was obtained by using dry toluene [48]. The glass beads are placed inside the solvent for several hours. SAMs are created on the surface.

The organofunctional group, which is dependent on the chosen silane, gives the surface different properties. Based on the experience of the Molecular Nanofabricationg Group of the University of Twente, we try to increase the adhesion by treating the glass with 11-cyanoundecyltrichlorosilane. The compete procedure can be read in Section 3.1. At the end of the procedure, we are left with an amine group, which is comparable to 3-amineopropyltriethoxysilane (APTES), but reacts slower with this hydroxy group on the surface and is less durable due to the longer chain. APTES is commonly used as an adhesion promoter between silica and an organometallic material. The question of how adhesive the glass beads are is determined in Chapter 4, in a single-contact study.

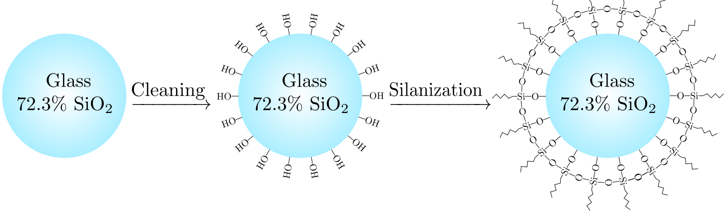

Figure 2.7: General procedure to create SAMs.

2.5.2 Previous particle modifications

Several silanes have been tried by others [9, 10, 11, 44]. The adhesion force these researchers measured are summarised in Table 2.2. The studies of Mäder et al. assumed the adhesion force is dependent on the applied load: the contact model 'stiff particles with soft contacts'. In this research the 'jump-in' force is measured. The other researchers measured the real pull-off force directly or indirectly. See Section 2.6, where the adhesion force measurements are summarised.

In Mäder's earliest study, she compared three different methods to determine the adhesion and found contradictory results [9]. The results for dimethyldichlorosilane showed a different adhesion force. This is due to different reaction times. If a monolayer is created, the reaction time does not influence the adhesion force significantly. Additionally, the adhesion force result of SigmaCote®are not consistent results. The adhesion force and the particle size does not show a correlation.

Table 2.2: Silanes tried by others. FPTS is 3,3,3-trifluoropropyl trimethoxysilane, CDMPS is chlorodimethylsilane and PFTOS is 1H,1H,2H,2H-perfluorooctyltriethoxysilane. Interface 1: untreated sphere touching a treated flat substrate, 2: treated sphere touching a flat steel substrate, 3: treated sphere touching a treated sphere and 4: a treated sphere against a treated substrate.

Silane	FPTS [9, 10]			CDMPS [9, 10]			PFTOS [9, 10]			
R_p [μm]	17.3	284.3	513.2	17.3	284.3	513.2	17.3	284.3	513.2	
F_ad [μN]	1.9	$4.03{\cdot}10^6$	$13.3{\cdot}10^6$	0.3	$4.95{\cdot}10^6$	$10.9{\cdot}10^6$	0.16	$4.56{\cdot}10^6$	$15.6{\cdot}10^6$	
Interface	1	2	2	1	2	2	1	2	2	
Silane	**Dimethyldichlorosilane [11]**			**SigamCote®[44]**						
R_p [μm]	850	850	850	66.4	63.8	59.8	53.0	47.5	42.3	37.3
F_ad [μN]	60	75	110	3.81	4.30	3.60	3.90	3.50	3.00	2.70
Interface	3	3	3	4	4	4	4	4	4	4

2.5.3 Polymerisation

Polymerisation is one of the risks when making a SAM. In this case, of a monolayer, agglomerations of silanes which reacted with water layer on the surface, or those that did not react, dry on the surface and later reacts with moisture in the air. Large clumps of silane polymers are unequally spread over the surface. Which depends on many process parameters [49]. The process and materials need to be under the same conditions to make a repeatable layer. Once there are agglomerations of silanes, the non-uniform layer results in statistical challenges.

Spots of polymerization can be identified with an atomic force microscope (AFM) topology pictures. Clumps of silanes with a height of a few tens of nanometers can be seen on the surface. For example, this occurred with the silanized beads produced by Mäder et al. [9]. Another indication can be read from the process steps. For example, in Jarray et al., the beads were taken out of the silane solution and left to air dry without first being rinsed with a dry solvent [11]. This allowed unreacted silanes, which were still present on the surface, to react with the moisture in the air, causing unequally distributed polymerised spots on the surface.

2.6 Adhesion force measurements

After the surface modification, the attractive force between the surfaces needs to be measured. There are several measuring methods compared by Israelachvili [25]. In total, he discussed nine methods, six of which use a liquid. Our interest is in measuring 'dry' cohesion between two solid surfaces, those three are shown in Figure 2.8. For spherical particles, the peeling method does not make sense. The other two methods are discussed here.

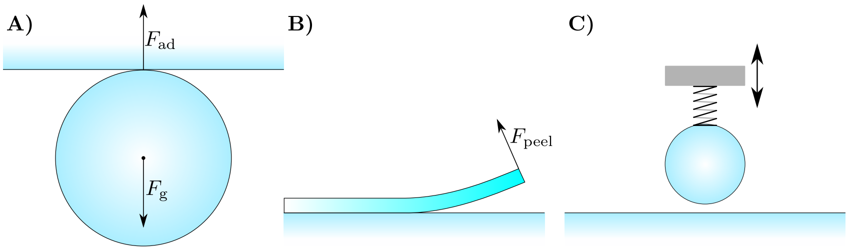

Figure 2.8: Three different adhesion force measurements: A) by direct pull-off, B) by peeling and C) by measuring the force–displacement response.

2.6.1 Adhesion force by pull-off

The adhesion force between two solids can be measured by bringing those bodies in contact and then pulling them apart. Mäder [10], Jarray [11] and Zafar [44] used this method to determine the adhesion of their silanized glass beads. Figure 2.9 shows the devices they used. Zafar and Jarray brought the bodies in contact with an unknown force. They needed to assume the adhesion force is independent on the applied load. For example, the contact model of JKR or DMT.

Mäder et al. placed a particle between two steel punches. One punches was connected to a spindle actuator with load cell and the other to a displacement sensor. When a spindle actuator applies a force on the particle, and afterwards unloaded. A force–displacement curve could be obtained. However, they measured with an applied load of several newton's, while the adhesion forces are in the range of several micro- or milinewtons depending on the particle properties[35]. If we back calculate the effective modulus of elasticity (Equation 2.4) for the unmodiefied glass bead with a flat glass–spherical glass interface, it is almost exactly a factor of ten off compared to the presented results. Mäder et al. are measured a glass–steel interface with adhesion forces on the order of several Newtons. This all indicates the device was not able to measure the adhesion correctly.

Jarray et al. brought two beads in contact and pulled them apart, ussing a glued rope. A micro balance was used to record the force. The contact unit direction needs to be in the pull direction to measure without tangential forces. How to obtain this for two spherical contacts is unknown. The measuring method seems to work quite well if the adhesion is independent of the applied load and when used to measure a bead in contact with a flat substrate.

Zafar et al. brought several polydisperse particles with a diameter in the range of 20–125μm in contact with a flat substrate. With the use of a microscope, an images was made of the particle sizes on the surface before the test. The substrate with the attached particles was dropped from a certain elevation and stopped rapidly. With a high-speed camera the impact velocity could be back calculated. Afterwards, another microscopic images was made to see which particle sizes detached. This was repeated for different elevations. The adhesion force was calculated with Newton's second law. This device is suitable if the adhesion is independent of the applied normal load, and the grain sizes are small.

2.6.2 Adhesion force–displacement curve

Another method to measure the adhesion is by making a force–displacement curve of the contact using a calibrated spring. An AFM is a well-known device for such a measurement. An AFM has a calibrated lever, the tip of which taps a surface, and the force and displacement of the tip are determined. For example, a surface roughness can be determined in nanoscale or to make a force–displacement graph. Those levers can be delivered with different tips or can be adjusted by the user to glue a bead at the end. An earlier study of Mäder et al. used an AMF to determine their adhesion [9]. Only small size particles can be used, due to the small forces and displacements. However, Fuchs et al. reported adhesion forces with a small error bar [40].

To determine the adhesion on beads of larger scales, a greater spring stiffness is required. Yaqoob used a lager device working with the same principles as the AFM [35]. A complete force–displacement curve of the contact was made, as well as the friction coefficient. This all took place in a chamber where the pressure and humidity can be controlled, since the effect of humidity has an influence on the adhesion.

Measuring the adhesion force–displacement response is preferred. The complete loading and unloading curve can be recorded, and a contact model can be chosen based on the measured responses. If the

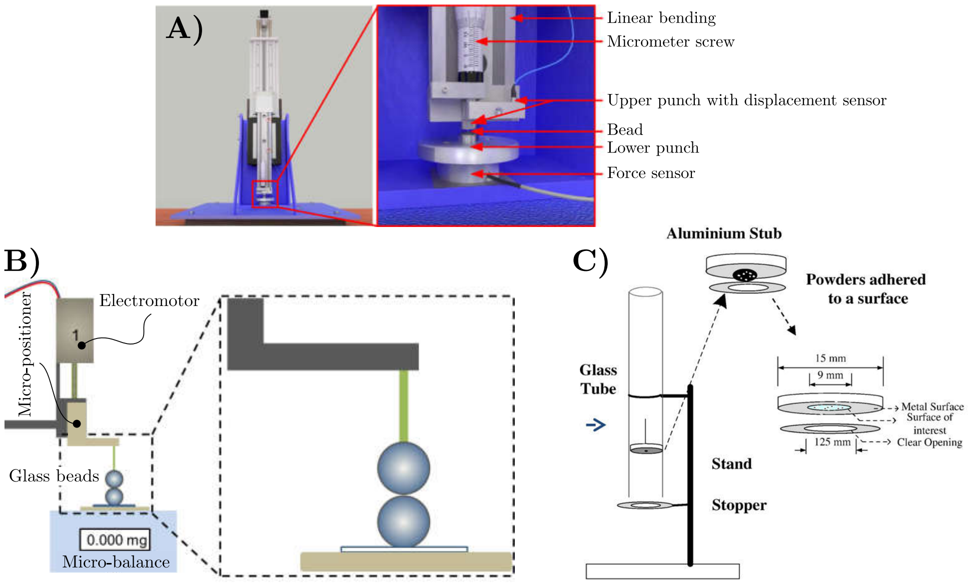

Figure 2.9: Adhesion force test setups of A) Mäder et al. [10], B) Jarray et al. [11] and C) Zafar et al. [44].

adhesion is dependent on the applied load, the maximum applied load can be extracted.

2.7 Micro to Macroscopic

Going from micro to macroscopic is challenging. All adhesion force models are determined for perfectly smooth surfaces, while soda-lime glass beads (Silibeads, Type S) have a mean surface roughness (RMS) in the range of 40–75nm [10]. The SAMs have a thickness of a few nanometers, depending on the chosen silane. Together the beads are not fully composed of silca oxide as mentioned before, islands of monolayer can be on the surface. And the silane can polymerise as well.

What a surface can look like after chemical treatment is shown by Mutua et al, who made a scanning electron microscope (SEM) image after treatment with APTES (see Figure 2.10) [50]. A monolayer is not observed here, but polymerised 'hairs' on the surface are. A monolayer is not visable in a SEM images, since it is only a few nanometers thick. A quote of prof.dr.ir. Jurriaan Huskens summarizes it well: "Silane chemistry is often tricky, usually more art than science, and procedures that may work well in one lab may not easily be reproduced in another".

Care and precision are required in the chemistry. After the chemistry, the surface needs to be checked. If the surface is not homogeneous, a statistical analysis needs to be performed.

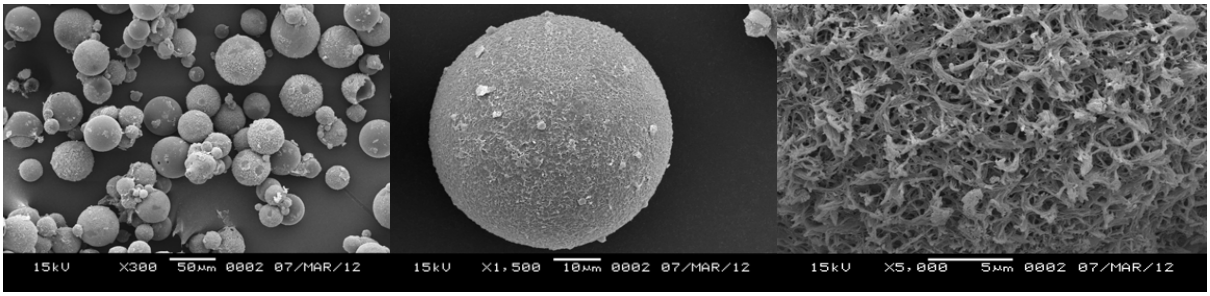

Figure 2.10: SEM images of glass beads after silanization [50]. Left: a couple of particles are shown. Middle: one bead. Right: a close up of the surface of a single bead.

3 Surface modification

In order to modify the surface of the glass, silanization is done. In this section the process we follow to functionalise the surface is described. Afterwards, several checks are done in order to determine if there is a layer on the glass.

3.1 Silanization procedure

To modify the surface of the glass beads, silanization is preformed. The explanation of the process can be read in Section 2.5.1. In this section, we describe the procedure we followed, which is based on early work of Onclin [51]. The procedure is slightly different, as we want to end with an amine group only. A calculation of how many beads could be treated with a silane can be found in Appendix B.

3.1.1 General procedure.

- All processes with moisture-sensitive chemicals were carried out in an argon environment.
- All chemicals were commercially bought and used as received. Table 3.1 lists the suppliers.
- All glassware used to prepare the monolayers was washed and afterwards cleaned with a large amount of Millipore water and dried in an oven.

Table 3.1: Suppliers of the chemicals used.

Chemical	Supplier	Amount
Sulfuric acid	VWR chemicals	–
Hydrogen peroxide	Merck	–
11-Cyanoundecyltrichlorosilane	abcr	5g
Red.Al.	Sigma-aldrich	–
Hydrogen chloride	–	–
Sodium hydrogen	–	–

3.1.2 Procedure to create the SAM.

1. Clean the glass beads and flat glass in freshly mixed piranha solution for at least 60 minutes. Piranha solution is made of a mixture of sulfuric acid H_2SO_4 (96%) and hydrogen peroxide H_2O_2 (30%) in the volume ratio 3:1.[1]
2. Flush the glass with a large amount of Millipore water, and dry in stream of nitrogen.
3. Expose glass to a cooled (3–7°C) 0.1-vol% solution of 11-cyanoundecyltrichlorosilane in freshly distillate toluene overnight.
4. Rinse glass with toluene to remove the unreacted silanes, and dry in a stream of nitrogen.

---

[1] Note: Piranha solution is a very strong oxidant, which reacts with organic substances.

5. Reduce the cyano-treated SAM to the corresponding amines by immersion for 4 hours in a 10-vol% solution of Red-Al®in toluene at 40°C. The amines will increase the cohesion.
6. Sonicate the glass in a 1M hydrogen chloride (HCl) solution for 5 minutes to remove aluminum salts.
7. Sonicate the glass again he material in a 0.5M sodium hydroxide (NaOH) solution to deprotonate the amines for 1 minute [52].

3.2 Layer characterisation

To determine if the glass surface was fully covered with the silane layer, we preformed several tests. For practical reasons, all these measurements were performed on flat microscope glass (Menzel-gläser). First, an infrared spectrum (FTIR) was made to determine which atoms were on the surface. Second, the contact angle was measured and compared with that of Onclin's work [51]. Third, scanning electron microscope (SEM) images were taken to see whether the surface had changed. Lastly, an atomic force microscope (AFM) topology picture was made of the surface.

3.2.1 FTIR spectrum measurement

FTIR stands for Fourier transfer infrared spectroscopy, which is a technique to measure the absorption or emission of a solid. Every molecule reflects with a different wavenumber ($\bar{\mathrm{v}}$). From the data, one can see what kinds of molecules are near the surface based on the change in absorption (α). Our layer should be noticeable in this measurement. One remark: since flat transparent glass was used, some infrared bundles were scattered inside the material. This meant we could not determine absolute numbers from the measurements. The used equipment was a Nicolet 6700 of Thermo Scientific.

The data is displayed in Figure 3.1, where indeed a cyano group can be noticed at 2,240cm^{-1}. This group has a weak amplitude and is partly in the background of the machine. We used an open environment FTIR, which means a background image was required to excluded the molecules of the air. The cyano group has a wavenumber almost comparable to that of carbon dioxide, which is present in the background. At 847cm^{-1} is a C-H bond, which is only in the treated samples [53]. The silanized glass (cyano and amine) gives a higher peak in the 2,800–3,000cm^{-1} region, attributed to symmetric and asymmetric C-H bonds in methylene groups [54]. This means there were some atoms of the silanes near the surface, but as mentioned infrared was scattered inside the glass, giving a result that is not very clear.

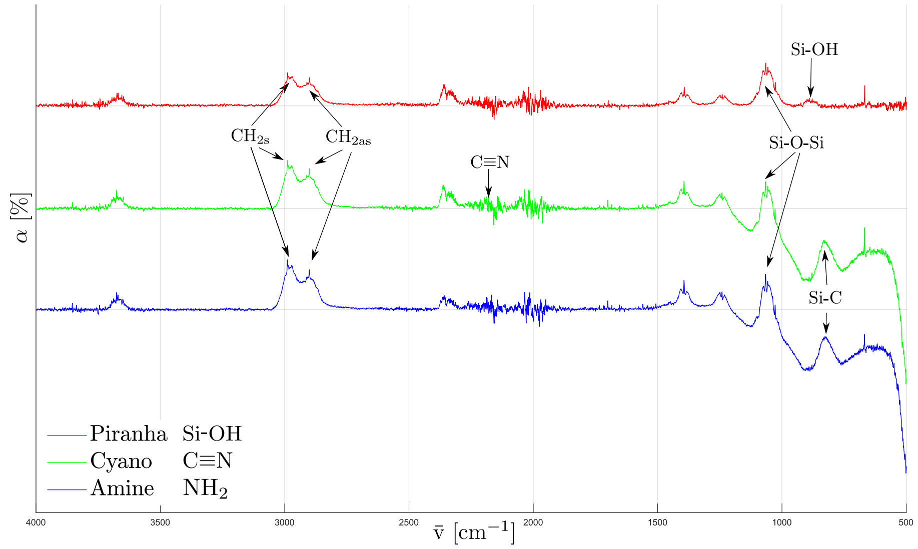

Figure 3.1: FTIR measurements of cleaned flat glass in piranha, silanized flat glass with a cyano end group and the reduced flat glass with an amine end group.

3.2.2 Contact angle measurement

Another method to determine if there is a dense layer, e.q., if the chemistry worked well, is by measuring the contact angle of a water droplet on the flat glass. If the layer is not dense, the contact angle will be smaller. Onclin did the same for his samples, such that we could compare results. Table 3.2 gives the contact angles. Good agreement between the angles is observed, meaning the chemistry is reproducible and comparable with Onclin's. Onclin's results showed a monolayer on a silicon wafer. The equipment used to measure our contact angle was a Krüss G10 with Millipore water as liquid. With the contact angle measurement, the surface energy can be back-calculated where ideally the contact angle of two different liquids are measured. However, Janssen et al. [55] measured the same contact angles as well and back-calculated the surface energy using the OWRK model, to a surface energy. and split in a dispersive energy (γ_D) and a polar energy (γ_P), $\gamma = \gamma_D + \gamma_P$ [56, 57]. The results are shown in Table 3.2 as well.

*Table 3.2: Contact angle results for advancing θ_a and receding θ_t. *Data from Mader et al. [9]*

SAM	Onlcin [51]		Our		Janssen [55]	Surface energies [9, 56, 57]		
	θ_a [°]	θ_t [°]	θ_a [°]	θ_t [°]	θ_a [°]	γ [mJ/m^2]	γ_D [mJ/m^2]	γ_P [mJ/m^2]
Piranha	-	-	170+		-	74.02*	39.83*	34.19*
CN	73±1	60±2	79±1	57±2	68.1±0.6	41.33	15.65	25.68
NH_2	60±1	25±2	61±1	35±2	58.4±1.7	45.25	30.73	44.12

3.2.3 SEM image

SEM images were made to see if there was a change on the surface after treatment. However, SEM images show only the surface texture, a monolayer cannot be detected, since the scale is to large and a gold layer was required. We were interested in how dense the layer was and that the surface was not polymerised. The cleaned flat glass surface (Piranha cleaned), silanized flat glass (Cyano group C≡N) and the reduced flat glass (Amine group NH_2) were prepared by placing in a vacuum oven at 80°C overnight and were afterwards coated with a gold layer using the JEOL JFC-1300 auto fine coater. The microscope used was the JSM-7200F.

The images are shown in Figure 3.2. A difference can be noticed on the surface. As expected, with clear cleaned glass, nothing could be noticed, although at 5,000x zoom a damaged spot could be seen. The images were made 48 hours after cleaning the glass with piranha.

When looking at the cyano group surface, some spot could be noticed, which were quite equally distributed over the surface. What these spots were is difficult to say. Between the silanization and the capture of the SEM images, 18 days had passed. During this time, the samples stayed in an oven where dust and other contamination could have been disposed on the surface.

A new batch was made following the complete procedure described in Section 3.1.2. Once finished, the reduced flat glass samples were immediately placed inside the vacuum oven. Once again there were some spots on the surface. These were not equally distributed over the surface, as could be seen at 40x zoom. When these spots were magnified, it appeared that the silane was polymerised. To prove this, an Oxford Instruments energy disperive spectroscopy (EDS) was preformed. With an EDS, the atoms near the surface were made visible. The contribution of gold was distracted, since it was artificially added to the surface. Figure 3.3 shows the analysis. As can be seen the spots consist more or less of carbon, which indicates the silane is polymerised. As mentioned before, a monolayer cannot be detected with SEM images.

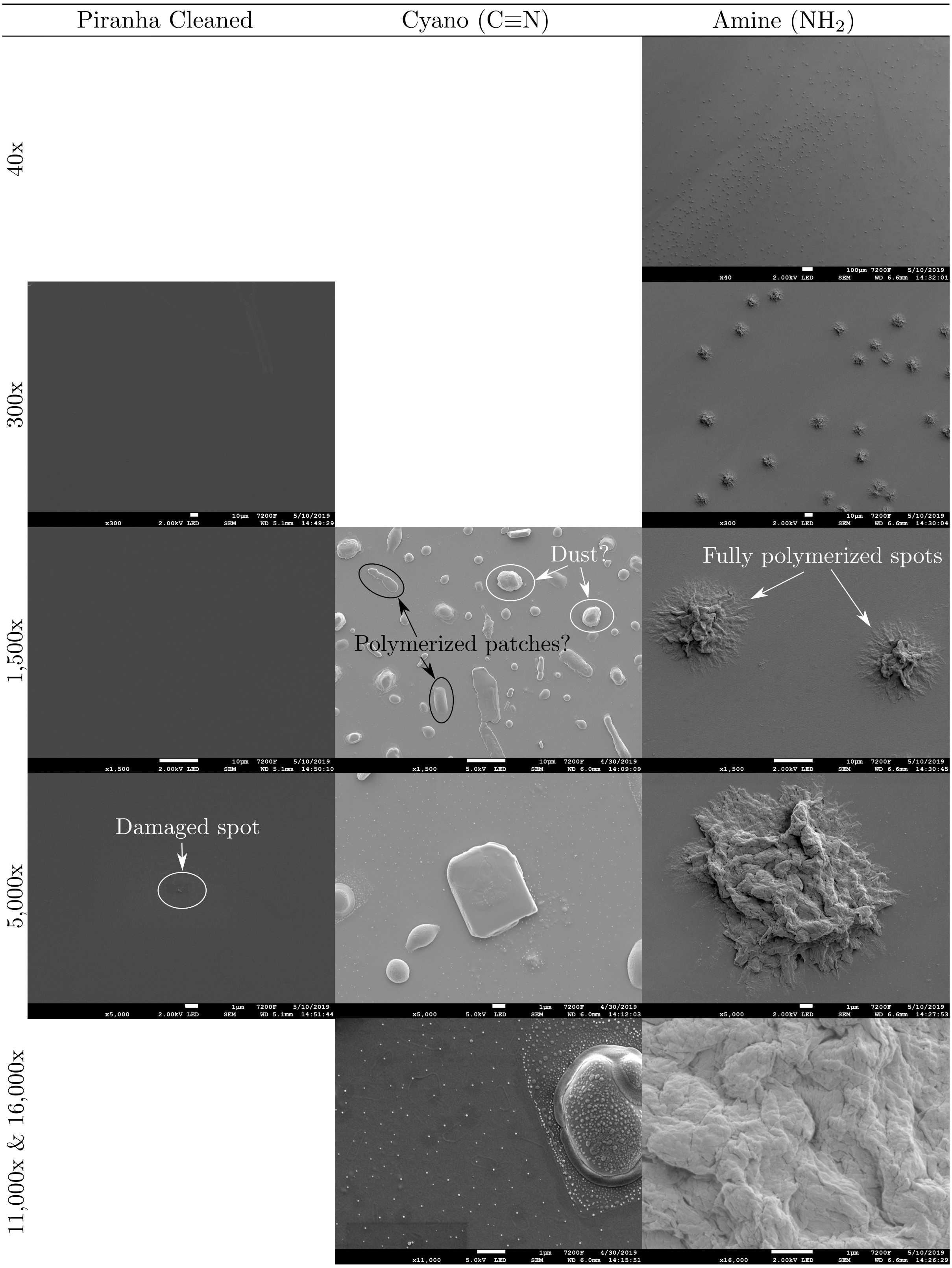

Figure 3.2: SEM images of the different silanization steps. Note that the pictures of the cyano group are not representative. Eighteen days elapsed between the chemistry steps and capturing of the images. Considerable contamination could have been deposed on the surface.

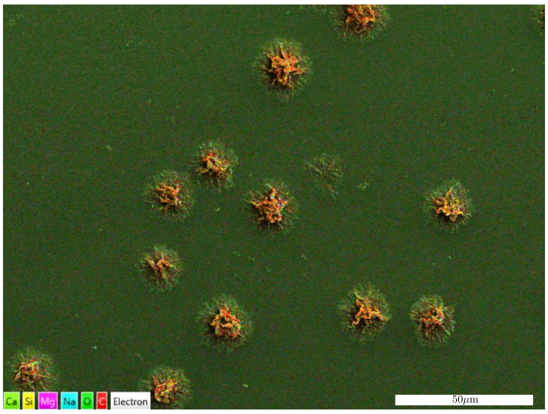

Figure 3.3: EDS picture of the amine glass surface.

3.2.4 AFM measurement

As the SEM images indicated polymerisation, an AFM topology picture was made to determine whether agglomerates of polymerised silanes were on the surface. Tapping mode AFM measurement was performed on the cleaned, silanized (cyano group C≡N) and reduced flat glass (amine group NH_2). A period of seven elapsed between the chemistry steps and the AFM measurement. During that time, all samples were kept in a closed petri dish made of glass to prevent contamination to the extent possible. The AFM used was the Veeco NanoScope V, with an Olympus OMCL-AC240TS tip. The surface roughness was determined as well with this measurement. A monolayer has the thickness of a few nanometers (2–10nm), depending on the length of a single chain, while a polymerised spot can have a thickness in the range of tens to a few hundred nanometers. The silane layer is soft, such that the layer spreads out due to the AFM tip.

Three 10 x 10μm^2 scans were performed on the same positions of every sample. The results are shown in Figure 3.4. The cleaned glass was measured at a damaged position, where scratches and contamination were noticed, which were not representative of the surface. Zooming into an undamaged area showed a more representative topology. On the cyano and amine surfaces, polymerised spots could be noticed. Agglomerates of silanes are unequally distributed over the substrate, especially in the cyano image. Zooming in to a sparsely polymerised area, the roughness decreased and only a few peaks could be noticed. After the reduction step (amine), there was a decrease in the thickness of the polymerised spots, but they were still there and not equally distributed over the surface. The AFM measurements showed indeed the samples were polymerised, even on the nano scale.

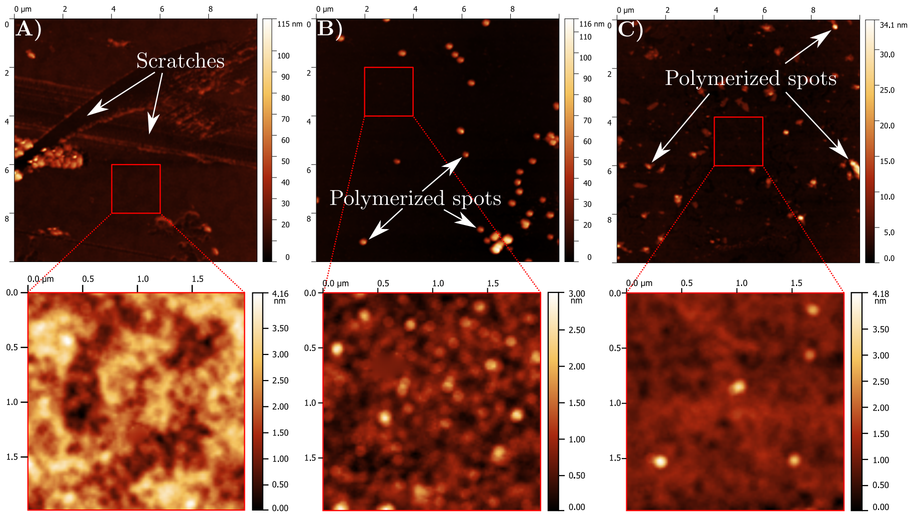

Figure 3.4: AFM images of A) cleaned glass B) silanized glass (cyano) and C) after the reduction stage (amine).

3.3 Discussion of surface modification

The surface of the glass was modified. In addition to a monolayer, agglomerates of polymerised silanes formed on the surface. These spots were unequally distributed over the surface. Trichlorosilane wants to react quickly with hydrogen. These polymerised patches are noticed on the flat glass samples, where drying is well controlled. For glass beads, cleaning and drying is even more difficult, such that the polymerised spots are even harder to prevent or control. Based on our research, polymerisation of silanes cannot be controlled such that a repeatable result cannot be obtained once polymerisation has occurred. Due to these unequally distributed agglomerates, statistical analysis needs to be performed to determine the adhesion force of a single contact, and the outcome is batch dependent. This wide variance appears in the results of earlier work of others [9, 10, 11]. An almost perfect monolayer is difficult to achieve. If the procedure is carried out under nitrogen, and the drying is done in an oven (where contamination of the surface is very likely), a better result might be obtained. Another method would be to switch to an alkoxy silane instead of a chloro silane. The alkoxy group is less reactive and thus less sensitive to moisture.

For the current, we used the treated (polymerised) batch to determine the adhesion of a single contact, while considering that the results are batch dependent.

4 Single-contact study

Once the beads were functionalised (monolayer with polymerised patches), the cohesion properties of a single contact was determined. We made use of the CMS Nano-Tribometer. With this device, the normal force and displacement are measured for unmodified glass and modified glass. Unmodified glass is glass as received and modified glass the complete chemical part is applied, the end group is the Amine (NH_2). The attractive forces can be extracted from these curves.

4.1 Force–displacement measurements

We used the CMS Nano-Tribometer, a machine developed to measure coulomb's friction coefficient for soft materials but will be used here for the normal load. Its normal load is and displacements are small (respectively in mN and μm range) compared with those of other machines. For this device, the Surface Technology and Tribology Group of the University of Twente made a program to measure the force–displacement of a single contact.

This program works as follows: The bead is almost brought in contact with the substrate by moving a spindle actuator in normal direction. A substrate is a flat glass sheet, modified when measuring a treated bead and unmodified when using a untreated glass pearl. The piezo actuator is controlled such that it moves as a cosine wave of one period (Figure 4.1 right). The amplitude (δ_{piezo}) and contact time (t) can be adjusted by the user. There are two displacement sensors, one at the piezo actuator itself and the other at the end of the calibrated spring (δ_{spring}). Before a measurement starts, the displacement of the spring was set to zero, $\delta_{\text{spring}} = 0$. The normal force of the bead is the displacement of the spring times the spring stiffness (k), $F_{\text{n}} = \delta_{\text{spring}} k$. The sum of the two displacements gives the displacement of the bead itself, $\delta = \delta_{\text{piezo}} + \delta_{\text{spring}}$. Figure 4.1 shows a schematic overview of the setup.

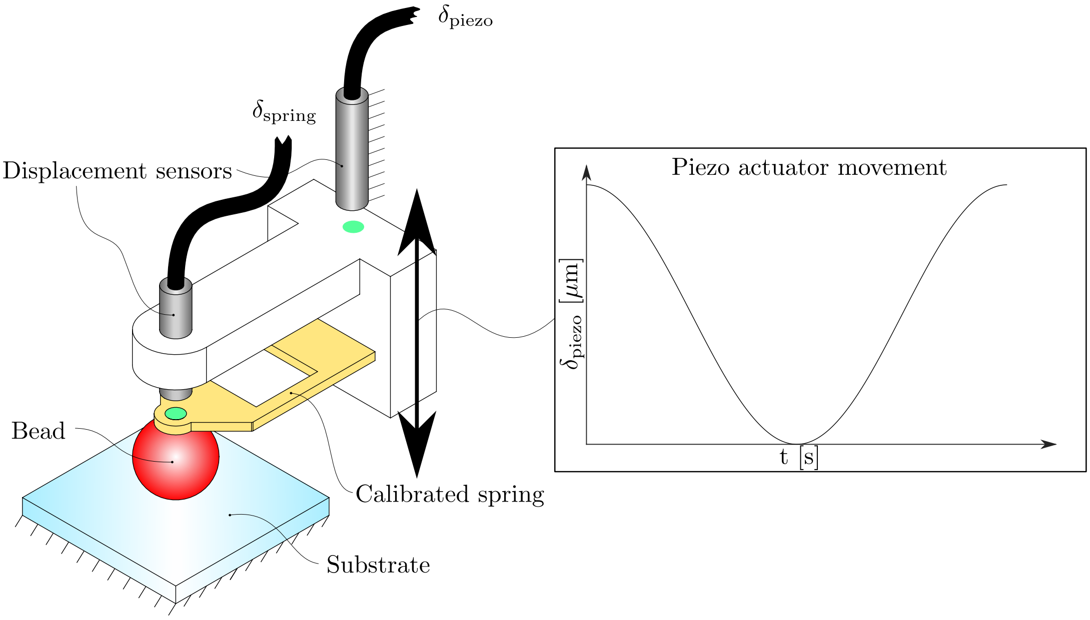

Figure 4.1: Schematic overview of the setup.

A typical measurement response is shown in Figure 4.2, where seven loading and unloading curves are illustrated, representing the first attempts to measure the adhesion of an unmodified glass bead in contact with flat glass. The curves are moved artificially. When a certain force was measured, this was recognized as the zero displacement point. The black line is the Hertzian of a glass ball, which was expected. As can be seen, the measured results are away from this line. Caused because the properties of the glue are also measured. Glue was used to attach the bead to the spring. It has an elastic mdulus of around the 1.3GPa and a Poisson's ratio of 0.4 [58]. The green line shows the Hertzian of the glue, which follows closely the measured results.

To avoid measuring the stiffness of the glue, some clamps were made, the spring was in direct contact with the bead. The steel machine has a much higher Young's modulus than does glass, respectively 210GPa and 70GPa. Thus, we are not measuring the stiffness of the construction itself. Figure 4.3 shows a response when the clamps were used. At the start of the graph, the Hertzian line is away from the measured results. This is contributed to the surface roughness and attractive forces. The threshold force according Greenwood and trip can not be calculated, the surface roughness of the bead was not know.

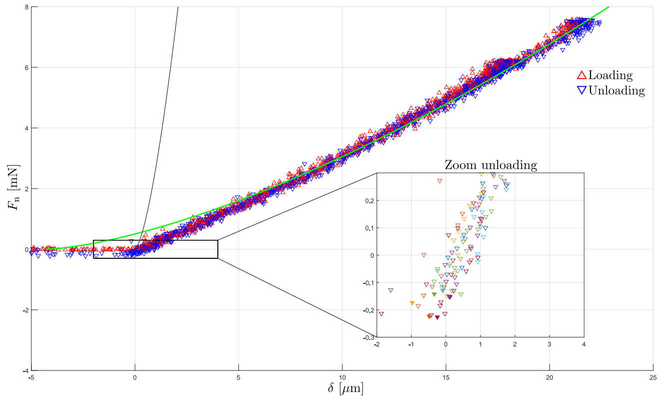

Figure 4.2: Force–displacement responses of a glued glass bead.

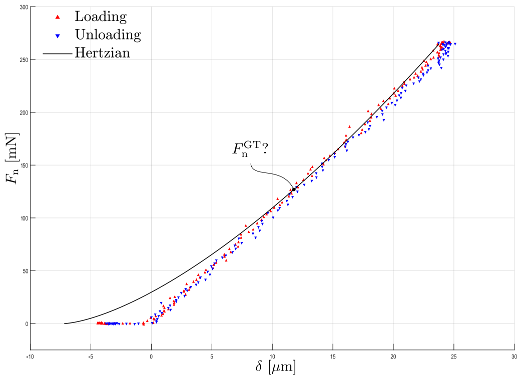

Figure 4.3: Force–displacement response of a clamped bead.

Due to the polymerisation of the silane, the measurement had to be repeated several times to be able to perform statistical analysis. Once a glass bead was clamped, the measurement was repeated 10 times at the same spot. After the 10 measurements, the same glass bead was moved with a distance of 250μm to another untouched point on the substrate, and the measurement wass repeated 10 times at that fresh spot. This sequence was repeated such that 10 new points on the substrate were touched, and the glass bead has touched the glass 100 times. In total five same-size, treated and untreated glass beads, were tested in this sequence. In total, we took 2000 measurements, 500 of one size of bead. The diameters of the beads are 4 and 6mm.

4.2 Results and discusion

The measurements showed an irregular response for adhesion, stiffness, loading and unloading curves. To understand how the layer behaves, several additional test are performed. In this section the responses of the 2000 measurements are summarised. Second, we assess whether there is a speed dependency. Third, we investigate the wear of the layer, and what happens when the normal load is increased. Finally, we summarise the adhesion is summarized and back-calculate the surface energy.

4.2.1 Force–displacement responses

Different contact behaviour were observed during the measurements (Figure 4.4).

A) Unmodified glass: The line follows closely the Hertzian line of glass except the start of the line, where the surface roughness plays a role, and the Hertz model did not assume an attractive force. In Appendix C are 100 measurements of the unmodified 4mm bead. The unloading curve is below the loading curve, due to hysteresis.

B) Treated glass beads: The loading curve is slightly below the Hertzian line for untreated glass. How much below is dependent on location and bead and is likely, dependent on how polymerised the bead and substrate are. This is shown in the unloading curve as well. The normal force (F_n) was kept as high as possible; in other words, the distance between the substrate and the glass bead was kept as small possible. The unloading curve can go to the points indicated with I to IV. Where these points are located on the graph is bead dependent. Why the unloading curve is reaches point IV is a matter still to be researched. The displacement here increases while the force decreases, which could be due to viscoelastic properties. The influence of velocity is investigated in Section 4.2.2. If the normal force is increased during the measurement of one bead, it seems the unloading curve moves from point I to point IV (Appendix E). The lower limit seems to have the same dimension. This is further investigated in Section 4.2.4, where the normal force is increased.

C) Treated glass bead at a highly polymerised spot: Over the course of 100 measurements, one treated glass bead gave results consistent with 'stiff particles with soft contacts' model proposed by Tomas [1]. This bead probably had a high polymerised contact point and was fresh (measured within 24 hours after chemical treatment). More tests with fresh beads were not possible with the available lab time. The other beads where tested after 72 hours. The loading curve had a stiffness comparable to glue. The unloading curve moves to the adhesion limit (slightly curved due to hysteresis), thereafter, moving back to the starting point. The difference between the Tomas model and the measurement results is that there are no discontinuities in the loading curve, and the unloading is move back to the starting point. It looks like the layer is self-healing, since tehe curves are repeatable. See Appendix F for the results of these measurements.

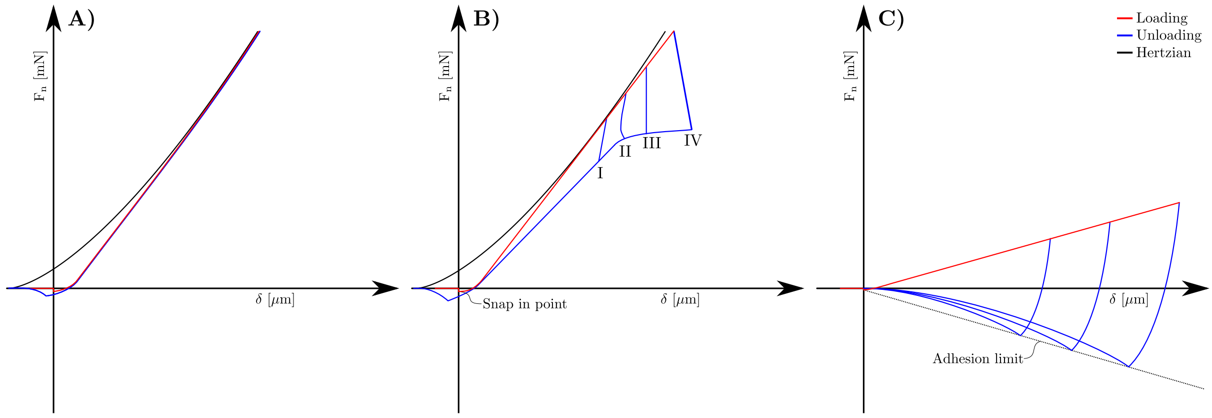

Figure 4.4: Summarised force–displacement responses of A) unmodified glass, B) treated glass and C) treated glass on at a highly polymerised spot.

4.2.2 Effect of contact time

The silanized glass may have viscoelastic properties, due to the presence of the polymers, indicating the time has an influence on the measuring results. Several measurements have been erased where the period of the cosine wave was changed (the contact time). A 4mm glass bead of medium cohesivity from the Jarray study was used [11] with a substrate of flat untreated glass. These beads were polymerised since, the unreacted silanes had 'dried' in normal air such that the remaining silanes could react with the moisture in the air and form cross links. A more polymerised bead should give a more clearly distinguishable difference if there is viscoelastic behaviour.

Figure 4.5 shows three set of results of each measurement. There are few differences between the responses. It was not possible to do experiments faster as 8 seconds. Speed appears to not have effect on the stiffnesses. However, from loading to unloading, the top is more flattened for the shorter measurement times. This is more noticeable in the results of the 10 second measurement as in the 8 second measurement.

An explanation could be layer wear and damage. The measurements were performed in the order of 10, 8 and 20 seconds without changing the contacting point. We were not able to measure on a fresh spot, since the huge change in response. In the next section, the influence of wear is investigated.

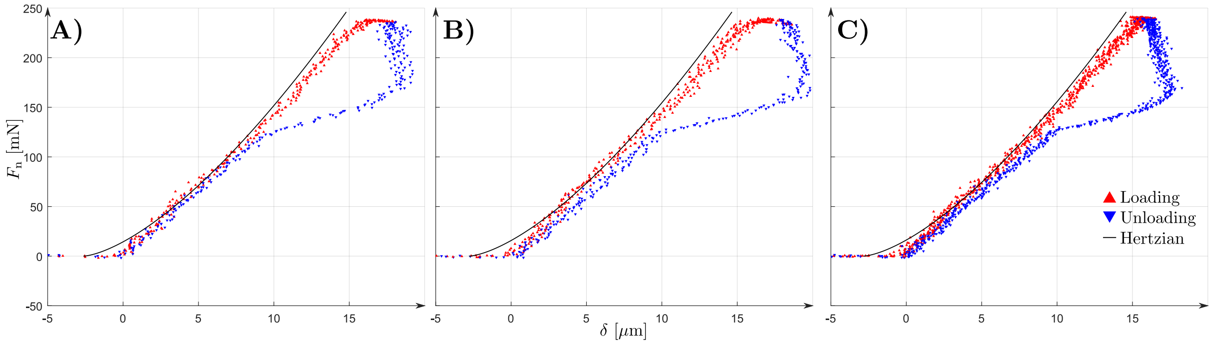

Figure 4.5: Responses for treated glass with different contact times: A) 8 second period (the quickest as possible), B) 10 second period (standard time) and C) 20 second period.

4.2.3 Wear of the layer

As mentioned in previous section, the layer was damaged by the number of collisions. This result was already noticeable in the first tests (Appendix D). In these results, the touching point on the substrate was changed after 10 contacts. It is probable that the substrate was less polymerised than the beads such that wear still could be noticed. During the chemical processing, it is more difficult to dry the beads than the flat glass. The measurement was repeated 150 times at the same contact point.

To show clearly the difference, movies were made of the first 50 measurements for the treated 4mm bead and a 6mm bead.[2] Figure 4.6 indicates the changes as well. The force–displacement graph is comparable to B in Figure 4.4, where the unloading curve is moves to point II for the 4mm bead and to point I for the 6mm bead. After approximately 25 measurements, the obtained results do not change significantly.

As can be seen, the loading curve becomes stiffer, indicating the layer is getting thinner or losing its elastic properties. The unloading curve has two stiffness slopes. The point at which they swap moves as the number of contacts increases, and it begins to stabilise after around 25 - 30 measurements.

To determine whether the layer had self-healing properties when it was at rest, the time between measurements was increased to 30 min. The results were comparable to earlier results.

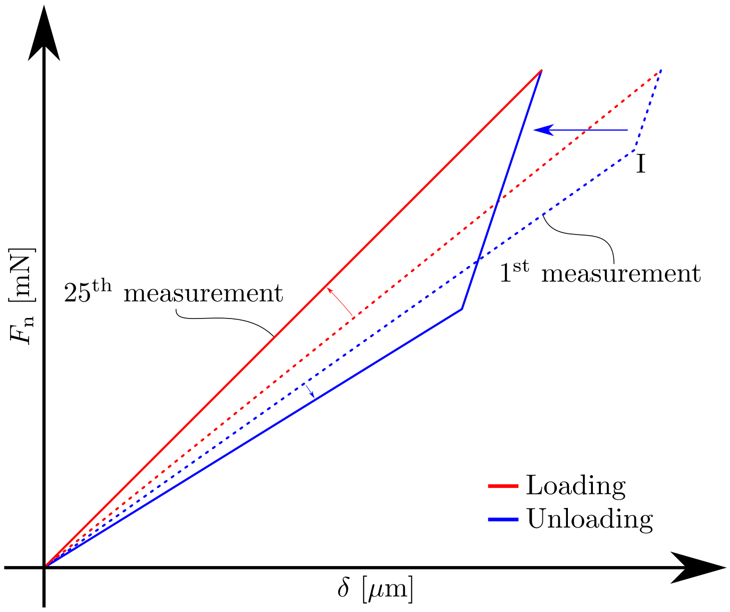

Figure 4.6: Wear of the layer (6mm treated bead).

---

[2] The movies can be viewed with the following links:
4mm bead: https://drive.google.com/file/d/1s_KbPXfspGdyVK5wuyTTxFGeULWJhEHx/view
6mm bead: https://drive.google.com/file/d/1nHPTG56tCjdCbgx7D7QZ42ciqgG5yPpK/view

4.2.4 Increase normal force

A few measurements showed a rounding in the top part of the curves, especially the beads from the Jarray et al. study [11] (Figure 4.5). To further investigate what was happening on the top part of the curves, the normal force needed to be increased. The amplitude of the piezo actuator was already at maximum displacement and the stiffest spring was used. To be able to increase the normal force, we brought the bead already in contact by using the spindle actuator. In this way, there was already a normal force applied before the measurement was started. An example what the displacement of the piezo (δ_{piezo}) looked for the first four measurements was summarised in Figure 4.7. This sequence was continued for 30 measurements. To exclude wear of the layer, the bead and substrate had previously been brought into contact. The measuring time was set to 60 seconds ensure numerous data points.

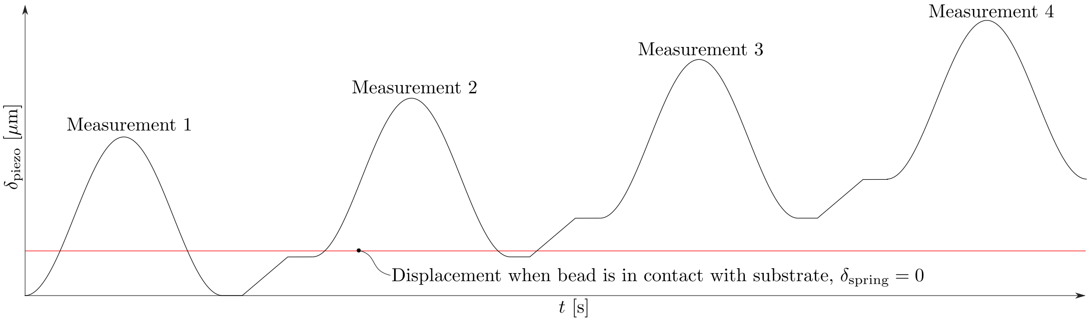

Figure 4.7: Displacement of the piezo element.

Figure 4.8 gives the matched force–displacement responses. The data were artificially moved to make the graph continues, since δ_{piezo} and δ_{spring} was set to zero before each measurement. The point when the force starts to increase was recognized as the bead was in contact with the substrate. By increase the normal load, a weaker stiffness was noticed. This bending point was used as fix point. The same was done when the stiffness starts to increase again. Appendix G presents the experimental setup.

In the beginning, the result is comparable with earlier results for B in Figure 4.4, with an unloading curve going to point IV. Quite early, the curvature at the top part is noticeable. When the bead was brought in contact, two loading stiffnesses were seen, the first slightly below the Hertzian of glass, and the second with a weaker stiffness. When a higher normal force was applied, there was a point at which the stiffness increased again with a stiffness farther below the Hertzian line. The unloading curve was almost the same as the loading curve, with the latter below the unloading curve due to hysteresis. When a measurement was started with a starting force between the 175 - 225mN, the displacement decreases with an increase of the normal load. In such a situation, the unloading behaviour is the same as the loading behaviour.

Why the unloading curve shows a weaker stiffness and then increases again is a matter still to be researched. It may be that the layer deforms plastically up to a maximum deformation point and the wants to follow the Hertzian line again, althrough with less stiffness because the contact area has increased, where the new layer parts need to be deformed as well. When unloading, the layer heals itself in a way that is repeatable. The explanation is doubt ful, since there is a 'plastic' deformation around the 40μm, while the layer is thinner than that.

4.2.5 Adhesion of silanized glass versus normal glass

The adhesion of all 2000 measurements is extracted from the force–displacement responses. We do not consider the adhesion of the response comparable to the 'stiff particles with soft contacts' model (Figure 4.4, C). In that case, the maximum adhesion is dependent on the applied normal force. In the other cases, the adhesion is independent of the applied load. We measured 500 force–displacement responses for every bead type. The adhesion force was extracted from the unloading curves by searching the minimum force, which is the pull-off force. The median and the median absolute deviation (MAD) were calculated for all the adhesion values. The humidity has an influence on the adhesion force, as described in Section 2.3.2. The lab was not humidity controlled.For consistency, we tried to measure under the smae constant conditions. For all tests, the humidity was known.

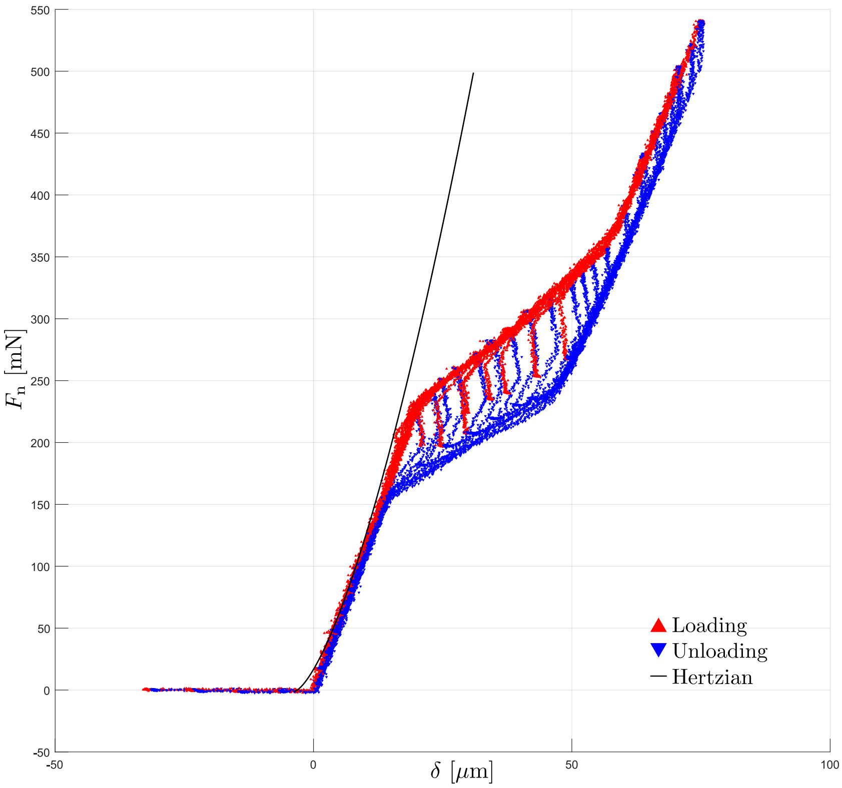

Figure 4.8: Responses when the load increases, for modified glass.

Table 4.1 gives the results of the extracted adhesion. As can be read, the adhesion for treated 4mm glass beads is lower than for normal glass, while the adhesion of 6mm silanized glass beads was higher than that of the unmodified beads. The results contradict each other. If we look for the differences in the experimental data set, the average humidity (RH_av) was the highest for the measurement of the clear 4mm glass beads. From models, we indeed see the adhesion is highly dependent on the RH [38]. Also, the average time (t_av) between the measurement and the chemical treatment was longer. Contamination and other dirt can negatively infleunce the results. However, Zafar found the silane coat does not age significantly [44]. If we are looking only to the results of the 6mm glass beads, we see the adhesion was increased roughly with 30% after treatment.

Testing at a highly polymerised spot or when the beads were very fresh increased the adhesion noticeably. The response was comparable to that predicted by Tomas 'stiff particles with soft contact' model [1].

Table 4.1: Adhesion force results.

	$F_\mathrm{ad}^\mathrm{ma}$ [mN]	MAD [mN]	t_av [days]	RH$_\mathrm{av}$ [%]
Glass 4mm	1.251	0.376	-	51.4
Treated glass 4mm	1.070	0.281	10.9	47.5
Glass 6mm	1.125	0.267	-	44.7
Treated glass 6mm	1.479	0.354	4.4	43.7

4.2.6 Surface energy

From the JKR and DMT theories, the work done by cohesion ($w = \gamma_{\mathrm{ss}}$) can be back-calculated from the cohesion force measured in Table 4.1 [20, 21].

$$\gamma_{\mathrm{ss}}^{\mathrm{JKR}} = \frac{2}{3}\frac{F_{\mathrm{ad}}}{\pi \bar{R}} \quad \text{and} \quad \gamma_{\mathrm{ss}}^{\mathrm{DMT}} = \frac{F_{\mathrm{ad}}}{2\pi \bar{R}} \tag{4.1}$$

The results are given in Table 4.2. These indicate that there is a difference between the surface energy for the two sizes of unmodified glass, while the surface energies for treated glass are quite simular. The errors are large, but still comparable to those of Yaqoob [35]. As defined in Section 2.2.5, the surface energy is equal to the work of adhesion ($\gamma_{\mathrm{ss}} = w = \gamma_1 + \gamma_2 - \gamma_{12}$), where the subscript 1 and 2 are the surface energies of the bodies in contact and subscript 12 is the interfacing energy between the materials.

Table 4.2: Calculated surface energies.

	F_{ad} [mN]	$\gamma_{\mathrm{ss}}^{\mathrm{JKR}}$ [mJ/m^2]	$\gamma_{\mathrm{ss}}^{\mathrm{DMT}}$ [mJ/m^2]
Glass 4mm	1.251±0.376	132.7±39.89	99.55±29.92
Treated glass 4mm	1.070±0.281	113.5±29.82	85.15±22.36
Glass 6mm	1.125±0.267	79.58±18.89	59.68±78.46
Treated glass 6mm	1.479±0.354	104.6±25.04	78.46±18.78

4.3 Dimensionless force–displacement graphs

All our measurements are with dimensions. To compare the results of two different tested beads, we make the force–displacement graphs dimensionless. The bead size then no longer matters. If the results scale well, the adhesion force can also be scaled. To do so, we need an equation with the units N and m. Since all our responses match quite closely to the Hertzian line, we make use of Equation 2.8, where the radius R and the equivalent Young's modulus (E^*) are material properties having the units m and N/m^2, respectively. These material properties are used to make the normal force and the displacement dimensionless. Starting with the displacement:

$$\bar{\delta} = \delta {E^*}^a R^b \quad \rightarrow \quad \bar{\delta} = \frac{\delta}{R}. \tag{4.2}$$

The same is done for the force:

$$\bar{F^{\mathrm{n}}} = F^{\mathrm{n}} {E^*}^a R^b \quad \rightarrow \quad \bar{F^{\mathrm{n}}} = \frac{F^{\mathrm{n}}}{R^2 E^*}. \tag{4.3}$$

With these dimensionless variables, several force–displacement graphs are made dimensionless; see Figure 4.9 for the results A) with dimensions and B) without. Graph A) with dimensions closely follows the Hertzian line, as already reported; only a small offset can be noticed. When making the graphs dimensionless, the maximum normal force is lower of the 6mm bead. This is because the force in Equation 4.3 is divided by the radius squared. There is also a slight difference in the slope. This could be the result of some difference in elastic modulus between the beads. In Figure 4.10, simalar graphs are made for the modified glass beads. The results matches with those obtained for unmodified glass beads.

Making the graphs dimensionless does not provide more insight into the layer behaviour or provide a result independent of the bead size.

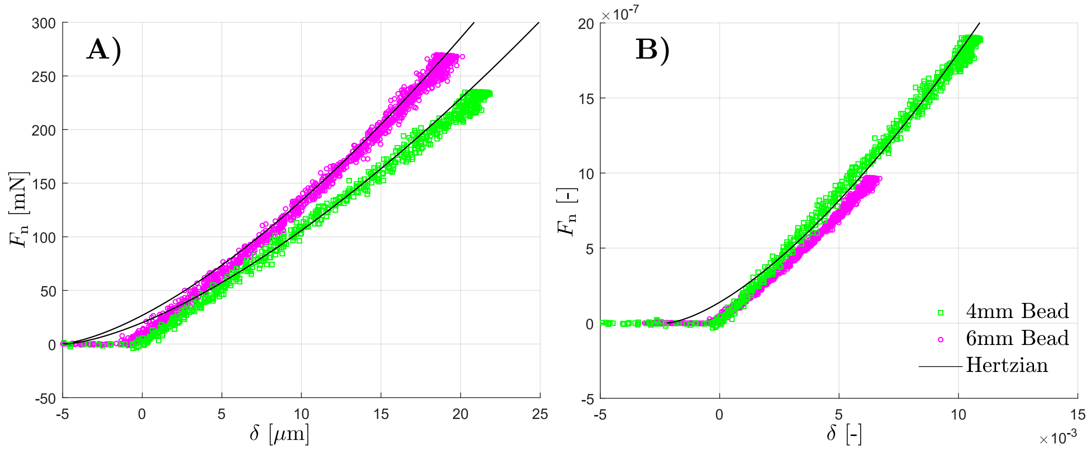

Figure 4.9: Force–displacement response of an unmodified glass bead: A) is with dimensions and B) without dimensions.

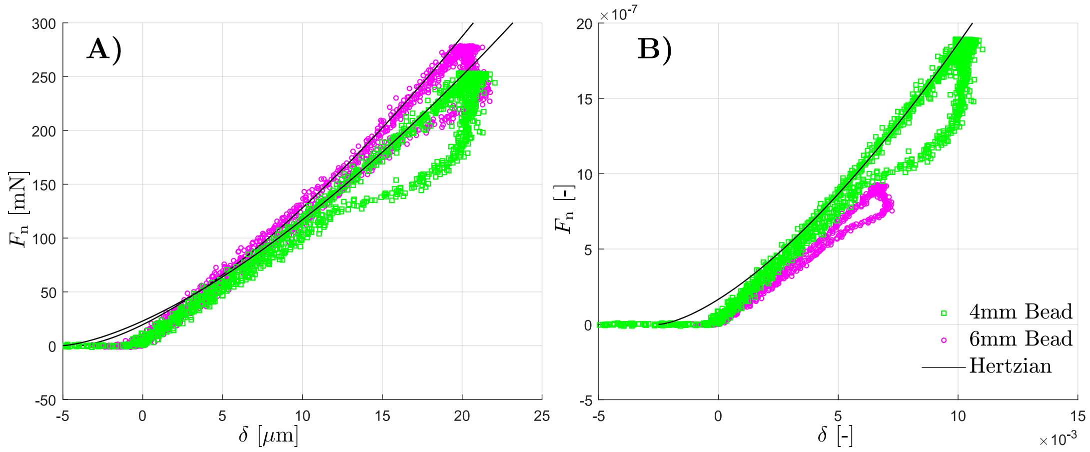

Figure 4.10: Force–displacement response of a modified glass bead: A) with dimensions and B) without dimensions.

5 Conclusion, discussion and recommendations

5.1 Conclusion and Discussion

Going from microscopic to macroscopic properties is challenging. All the contact and adhesion models are derived for smooth surfaces, but in real applications, the surface is always rough. Additionally, the humidity in the room several layers of water around the bead. This is changes the cohesion or adhesion between the bodies, as capillary forces are in play between the asperities.

The method to make the glass beads cohesive, silanization, turned out to be moisture sensitive. Agglomerates of silanes chains are unequally distributed over the surface, as can be seen on the SEM images and AFM topology pictures (Figures 3.2 and 3.4). Those measurements are performed on flat glass, which is easier to dry compared then glass beads. It is likely the glass beads have more and lager unequally distributed polymerised spots across the surface, thus the beads give different responses, depending on the location of contact.

The Nano-Tribometer is an ideal device to measure the force–displacement response of a single contact on the macroscopic scale. Unmodified glass beads gave a result which is comparable to the Hertzian line of glass, except in the low loading range, where surface roughness and adhesion effects play a role. The Hertz model does not assume those. Since we were measuring at low loading ranges, environmental vibrations are within the results, giving an adhesion force with a large error range (±30%). The same holds for measuring at different humidity levels. Ideally, the device needs to be placed on an active vibration isolation table in a humidity-controlled room to measure a more accurate adhesion force.

As expected, the modified glass beads showed irregular behaviour, due to polymerisation of the silanes. The response is dependent on the contact point, making it difficult to predict their force–displacement response. In such cases a highly polymerised spot is highly adhesive and has a response comparable to the models in the literature [1, 23]. Another explanation could be that the measurements were performed within 24 hours after chemical treatment. However, the measured stiffness was much lower than the Hertzian of glass, meaning it was more probable that a thick patch of silanes was contacted.

In most cases, the modified glass beads gave a force–displacement response never seen before (B in Figure 4.4). The curves can go to the point I to IV and thereafter move almost back to the previous loading curve. In particular, it is not clear when the curve is going to the point IV is not clearly understood. It seems the layer does not have viscoelastic properties. If the speed of the measurement is changes. A recommendation is to measure with a period of at least one hour to see if there are really non viscus effects. Increasing the normal force gave after an applied load a weaker stiffness. Indicating the layer deforms plastic. Once the layer is fully plastic deformed the stiffness is again comparable with the Hertzian. Unloading follows the same curve but under need the loading curve due to hysteresis. The layer may have self-healing properties. Once the layer starts to deform plastic the displacement increases while unloading the force. Stopping when the layer is not fully self-healed, and loading again gives first a decrease in the displacement. This behaviour is not understood. A molecular dynamic simulation needs to be taken into account. A reason could be due to bridging of the layer, see Figure 2.10. Those bridges needs to be pushed in which happens after a certain load, thereafter a weaker stiffness is measured due to collapsing. Stopping at that load regime the bridges are still collapsing, giving an increase in displacement while unloading. After fully collapsing the stiffness is slightly below the Hertzian of glass again. When unloading the bridges wants to spring back to their initial shape (Self-healing). To see how the polymerised surface of the beads look like, it is recommended to make SEM images of the beads itself as well. After around 30 contracts, the increase in displacement while decreasing the load is not shown any more (treated 4mm bead). However, to clearly investigate the measurements need to be done with a stiffer spring.

When only looking to the 6mm beads, the cohesion is increased with roughly 30%. However, there is a big error in those adhesion values. A thick patch of silanes increases the adhesion a lot, while more or less a monolayer does not.

Can chemical silanization be applied to make glass beads controllably cohesive on the macroscopic scale? Silanization can be controlled when there is no moisture involved in the chemical process and all the glass is dry. A monolayer will be formed on the surface. However, this monolayer does not significantly increase the adhesion. The roughness of the beads are much larger as the thickness of the layer. Ideally, a thick soft layer is around the bead.

5.2 Recommendations

Using beads with a smoother surface is highly recommended, for example, silica or silicon beads. The effect of SAM could be more noticed and the polymerisation could maybe better be controlled. Still those surfaces has a certain roughness where a small change can influence the results [35].

Use an alkoxy silane instead a cholor silane. The alkoxy group is less reactive, which can help to prevent polymerisation.

Make SEM and AFM pictures of the beads before and after chemical silanization. The degree of polymerisation could be determined. As well the surface roughness.

To make beads cohesive, coat the particles with a thick soft porous layer. The contacting area will increase a lot to have more van der Waals forces. By making the layer porous, water can condense in the layer to get capillarity forces as well.

Preform the adhesion measurement in a humidity controlled lab and use a vibration isolation platform. The adhesion is depending on the RH, it is important to measure with the same conditions. The measured forces are small where vibrations having a influence.

To measure the viscoelastic properties, a force–displacement response needs to be done on a larger time scale. Preforming a measurement in at least one hour would be recommended.

Bibliography

[1] J. Tomas. Fundamentals of cohesive powder consolidation and flow. *Granular Matter*, 6(2):75–86, Oct 2004.

[2] R.L. Brown and J.C. Richards. Chapter 1 - introduction. In R.L. Brown and J.C. Richards, editors, *Principles of Powder Mechanics*, pages 1 – 12. Pergamon, 1970.

[3] J.C. Williams. The segregation of particulate materials. a review. *Powder Technology*, 15(2):245 – 251, 1976.

[4] J.M.N.T. Gray and A.R. Thornton. A theory for particle size segregation in shallow granular free-surface flows. *Proceedings of the Royal Society A: Mathematical, Physical and Engineering Sciences*, 461(2057):1447–1473, Aug 2005.

[5] B. Marks, P. Rognon, and I. Einav. Grainsize dynamics of polydisperse granular segregation down inclined planes. *Journal of Fluid Mechanics*, 690:499–511, 2012.

[6] D.R. Tunuguntla, O. Bokhove, and A.R. Thornton. A mixture theory for size and density segregation in shallow granular free-surface flows. *Journal of Fluid Mechanics*, 749:99–112, 2014.

[7] T. Shinbrot, A. Alexander, M. Moakher, and F.J. Muzzio. Chaotic granular mixing. *Chaos: An Interdisciplinary Journal of Nonlinear Science*, 9(3):611–620, 1999.

[8] S. Schmelzle and H. Nirschl. Dem simulations: mixing of dry and wet granular material with different contact angles. *Granular Matter*, 20(2):19, Feb 2018.

[9] K. Mader-Arndt, Z. Kutelova, R. Fuchs, J. Meyer, T. Staedler, W. Hintz, and J. Tomas. Single particle contact versus particle packing behavior: Model based analysis of chemically modified glass particles. *Granular Matter*, 16:359–375, 06 2014.

[10] K. Mader-Arndt, S. Aman, R. Fuchs, and J. Tomas. Contact properties determination of macroscopic fine disperse glass particles via compression tests in normal direction. *Advanced Powder Technology*, 28(1):101 – 114, 2017.

[11] A. Jarray, H. Shi, B.J. Scheper, M. Habibi, and S. Luding. Segregation in dry cohesive granular systems. -, page 1–13, Unpiblished jet.

[12] H. Henein, J.K. Brimacombe, and A.P. Watkinson. Experimental study of transverse bed motion in rotary kilns. *Metallurgical Transactions B*, 14(2):191–205, Jun 1983.

[13] J. Mellmann. The transverse motion of solids in rotating cylinders—forms of motion and transition behavior. *Powder Technology*, 118(3):251 – 270, 2001.

[14] J. Mosby, S.R. de Silva, and G.G. Enstad. Segregation of particulate materials – mechanisms and testers. *KONA Powder and Particle Journal*, 14:31–43, 1996.

[15] S. T. Nase, W.L. Vargas, A.A. Abatan, and J.J. McCarthy. Discrete characterization tools for cohesive granular material. *Powder Technology*, 116(2):214 – 223, 2001. Modelling and Computational analysis of a collection of particulate and fluid-solid flow problems.

[16] H. Li and J.J. McCarthy. Controlling cohesive particle mixing and segregation. *Phys. Rev. Lett.*, 90:184301, May 2003.

[17] M. Capece, R. Ho, J. Strong, and P. Gao. Prediction of powder flow performance using a multi-component granular bond number. *Powder Technology*, 286:561 – 571, 2015.

[18] J. Tomas. Pmechanics of particle adhesion, 2006.

[19] H. Hertz. Ueber die berührung fester elastischer körper. *Journal für die reine und angewandte Mathematik*, 92:156–171, 1882.

[20] K.L. Johnson, K. Kendall, and A.D. Roberts. Surface energy and contact of elastic solids. *Proceedings of The Royal Society A: Mathematical, Physical and Engineering Sciences*, 324:301–313, 09 1971.

[21] B.V. Derjaguin, V.M. Muller, and Y.P. Toporov. Effect of contact deformations on the adhesion of particles. *Journal of Colloid and Interface Science*, 53(2):314 – 326, 1975.

[22] V.M. Muller, B.V. Derjaguin, and Y.P. Toporov. On two methods of calculation of the force of sticking of an elastic sphere to a rigid plane. *Colloids and Surfaces*, 7(3):251 – 259, 1983.

[23] S. Luding. Cohesive, frictional powders: contact models for tension. *Granular Matter*, 10(4):235, Mar 2008.

[24] B. Dahneke. The influence of flattening on the adhesion of particles. *Journal of Colloid and Interface Science*, 40(1):1 – 13, 1972.

[25] J.N. Israelachvili. *Intermolecular and surface forces.* Academic Press is an imprint of Elsevier, 2012.

[26] K.L. Johnson and J.A. Greenwood. An adhesion map for the contact of elastic spheres. *Journal of Colloid and Interface Science*, 192(2):326 – 333, 1997.

[27] D. Tabor. Surface forces and surface interactions. *Journal of Colloid and Interface Science*, 58(1):2 – 13, 1977. International Conference on Colloids and Surfaces.

[28] R. J. Colton. Nanoscale measurements and manipulation. *Journal of Vacuum Science & Technology B: Microelectronics and Nanometer Structures*, 22(4):1609, 2004.

[29] M.A. R.S. Bradley. Lxxix. the cohesive force between solid surfaces and the surface energy of solids. *The London, Edinburgh, and Dublin Philosophical Magazine and Journal of Science*, 13(86):853–862, 1932.

[30] R.L. Brown and J.C. Richards. Chapter 4 - measurement of powder properties. In R.L. Brown and J.C. Richards, editors, *Principles of Powder Mechanics*, pages 82 – 115. Pergamon, 1970.

[31] J. Tomas and S. Kleinschmidt. Improvement of flowability of fine cohesive powders by flow additives. *Chemical Engineering & Technology*, 32(10):1470–1483, 2009.

[32] H. Krupp. Particle adhesion theory and experiment. *Advances in Colloid and Interface Science*, 1(2):111 – 239, 1967.

[33] L. Bergström. Hamaker constants of inorganic materials. *Advances in Colloid and Interface Science*, 70:125 – 169, 1997.

[34] C.M. Mate. *Tribology on the small scale a bottom up approach to friction, lubrication, and wear.* Oxford University Press, 2008.

[35] M.A. Yaqoob. *Adhesion and friction in single asperity contact.* PhD thesis, University of Twente, Netherlands, 12 2012.

[36] H.J. Butt, K. Graf, and M. Kappl. *Physics and Chemistry of Interfaces.* Physics textbook. Wiley, 2006.

[37] D.B. Asay and S.H. Kim. Evolution of the adsorbed water layer structure on silicon oxide at room temperature. *The Journal of Physical Chemistry B*, 109(35):16760–16763, 2005. PMID: 16853134.

[38] M.A. Yaqoob, M. Rooij, and D.J. Schipper. On the transition from bulk to ordered form of water: A theoretical model to calculate adhesion force due to capillary and van der waals interaction. *Tribology Letters*, 49, 03 2013.

[39] D.L. Liu, J. Martin, and N.A. Burnham. Optimal roughness for minimal adhesion. *Applied Physics Letters*, 91(4):043107, 2007.

[40] R. Fuchs, T. Weinhart, J. Meyer, H. Zhuang, T. Staedler, X. Jiang, and S. Luding. Rolling, sliding and torsion of micron-sized silica particles: experimental, numerical and theoretical analysis. *Granular Matter*, 16(3):281–297, Jun 2014.

[41] McFarlane J.S. and Tabor D. Adhesion of solids and the effect of surface films. *Proceedings of the Royal Society of London. Series A. Mathematical and Physical Sciences*, 202(1069):224–243, Jul 1950.

[42] J. Greenwood and J.B.P.P. Williamson. Contact of nominally flat surfaces. *Proceedings of the Royal Society of London (A)*, 295:300–319, 12 1966.

[43] J.A. Greenwood and J.H. Tripp. The elastic contact of rough spheres. *Journal of Applied Mechanics*, 34, 01 1967.

[44] U. Zafar, C. Hare, A. Hassanpour, and M. Ghadiri. Drop test: A new method to measure the particle adhesion force. *Powder Technology*, 264:236 – 241, 2014.

[45] B. Arkles. Silane coupling agents, 2014.

[46] K. Jradi, C. Daneault, and B. Chabot. Chemical surface modification of glass beads for the treatment of paper machine process waters. *Thin Solid Films*, 519(13):4239 – 4245, 2011.

[47] K. Mader-Arndt, Z. Kutelova, and J. Tomas. *Microscopic Particle Contact Adhesion Models and Macroscopic Behavior of Surface Modified Particles*, chapter 3, pages 105–155. John Wiley & Sons, Ltd, 2015.

[48] M.E. McGovern, K.M.R. Kallury, and M. Thompson. Role of solvent on the silanization of glass with octadecyltrichlorosilane. *Langmuir*, 10(10):3607–3614, 1994.

[49] J.A. Howarter and J.P. Youngblood. Optimization of silica silanization by 3-aminopropyltriethoxysilane. *Langmuir*, 22(26):11142–11147, 2006. PMID: 17154595.

[50] F. Mutua, P. Lin, J. Koech, and Y. Wang. Surface modification of hollow glass microspheres. *Materials Sciences and Applications*, 03:856–860, 01 2012.

[51] S. Onclin. *A molecular printboard on glass*. PhD thesis, University of Twente, Netherlands, 10 2004.

[52] M.T. Lee and G.S. Ferguson. Stepwise synthesis of a well-defined silicon (oxide)/polyimide interface. *Langmuir*, 17(3):762–767, 2001.

[53] N.D. Hegde, H. Hirashima, and A.R. Venkateswara. Two step sol-gel processing of teos based hydrophobic silica aerogels using trimethylethoxysilane as a co-precursor. *Journal of Porous Materials*, 2007.

[54] S. Armini, J. Loyo P., M. Krishtab, J. Swerts, P. Verdonck, J. Meersschaut, T. Conard, M. Blauw, H. Struyf, and M. Baklanov. Pore sealing of k 2.0 dielectrics assisted by self-assembled monolayers deposited from vapor phase. *Microelectronic Engineering*, 120:240–245, 05 2014.

[55] D. Janssen, R. de Palma, S. Verlaak, P. Heremans, and W. Dehaen. Static solvent contact angle measurements, surface free energy and wettability determination of various self-assembled monolayers on silicon dioxide. *Thin Solid Films*, 515(4):1433 – 1438, 2006.

[56] D.K. Owens and R.C. Wendt. Estimation of the surface free energy of polymers. *Journal of Applied Polymer Science*, 13(8):1741–1747, 1969.

[57] D.H. Kaelble. Dispersion-polar surface tension properties of organic solids. *The Journal of Adhesion*, 2(2):66–81, 1970.

[58] H. Cease, P.F. Derwent, H.T. Diehl, J. Fast, and D. Finley. Measurement of mechanical properties of three epoxy adhesives at cryogenic temperatures for CCD construction. -, 2006.

A Derivation JKR - Model

In Section 2.2.2 there is missing a derivation going from Equation 2.9 to 2.10. The derivation is done here:

$$\frac{4}{3}\frac{E^*}{\bar{R}}a^3 = F_\mathrm{n} + 3\gamma_\mathrm{ss}\pi\bar{R} + \sqrt{6\gamma_\mathrm{ss}\pi\bar{R}F_\mathrm{n} + \left(3\gamma_\mathrm{ss}\pi\bar{R}\right)^2} \tag{A.1}$$

$$\left(\frac{4}{3}\frac{E^*}{\bar{R}}a^3 - F_\mathrm{n} - 3\gamma_\mathrm{ss}\pi\bar{R}\right)^2 = 6\gamma_\mathrm{ss}\pi\bar{R}F_\mathrm{n} + \left(3\gamma_\mathrm{ss}\pi\bar{R}\right)^2 \tag{A.2}$$

$$\left(\frac{4}{3}\frac{E^*}{\bar{R}}a^3\right)^2 - \frac{8}{3}\frac{E^*}{\bar{R}}F_\mathrm{n}a^3 + F_\mathrm{n}^2 - 8E^*\gamma_\mathrm{ss}\pi a^3 = 0 \tag{A.3}$$

$$\left(F_\mathrm{n} - \frac{4}{3}\frac{E^*}{\bar{R}}a^3\right)^2 = 8E^*\gamma_\mathrm{ss}\pi a^3 \tag{A.4}$$

$$F_\mathrm{n}^\mathrm{JKR} = \frac{4}{3}\frac{E^*}{\bar{R}}a^3 - \sqrt{8E^*\gamma_\mathrm{ss}\pi a^3} \tag{A.5}$$

With $a \approx \sqrt{\bar{R}\delta}$ we derive:

$$F_\mathrm{n}^\mathrm{JKR}(\delta) = \frac{4}{3}E^*\sqrt{\bar{R}}\delta^{3/2} - \sqrt{8E^*\gamma_\mathrm{ss}\pi(\bar{R}\delta)^{3/2}} \tag{A.6}$$

Note: in Equation A.5 the last therm could have a plus sign as well. However, this therm is added due to adhesion which is always negative.

B Calculation of volume beads which can be treated with an amount of silane

Here is shown how to calculate the volume of particles which can be treated with a given amount of silanes. The used silanes is 11-Cyanoundecyltrichlorosilane, which has a molecular mass of 314.76g/mol.[3] The amount used for this experiment is 5g with a purity of 95%.[4] The amount of mols inside the substance is:

$$Nr_{\text{mols}} = \frac{\text{amount}}{\text{moleculair mass}} = \frac{5\cdot 95\%}{314.76} = 0.0151\text{mol} \tag{B.1}$$

With Avogadro's constant the amount of molecules can be calculated within 1 mol. The constant is N_A=6.0221486$\cdot 10^{23}$mol^{-1}.

$$Nr_{\text{molecules}} = Nr_{\text{mols}}\cdot N_A = 0.0151\cdot 6.0221486\cdot 10^{23} = 9.088\cdot 10^{21}\text{molecules} \tag{B.2}$$

To know how many silica (Si) atoms are at the surface of glass, we make use of a scanning tunneling microscopic image see Figure B.1.[5] The number of silica atoms are counted, which is 203. The microscopic picture has a size of 8×3nm^2. Giving 8.45atoms/nm^2 silica atoms on a square nanometre, which is equivalent to 8.45$\cdot 10^{12}$atoms/mm^2.

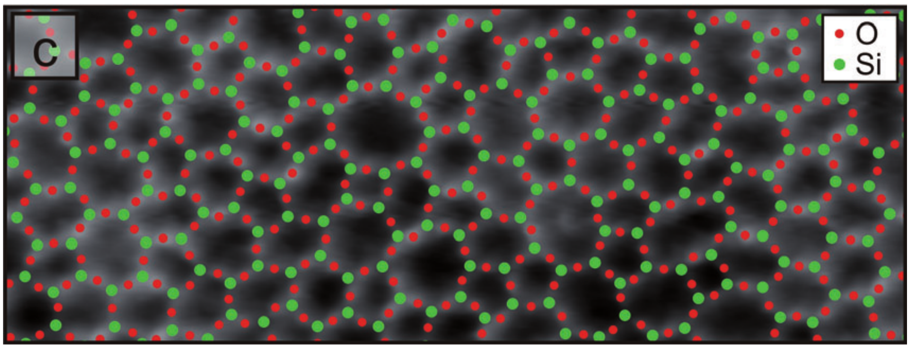

Figure B.1: STM image of glass surface

For this calculation we use a average sphere radius of R_s=20$\cdot 10^{-3}$mm, which is equal to 20μm. The area of one sphere can be calculated with

$$A_{\text{sphere}} = 4\pi R_s^2 = 4\pi 20\cdot 10^{-3^2} = 5.0\cdot 10^{-3}\text{mm}^2 \tag{B.3}$$

The total amount of silica atoms can be calculated by multiplying the numbers of atoms per square millimetre by the area of the sphere, which is 42.5$\cdot 10^9$ atoms per particle. When assuming all the silanes molecules are reacting with those of silica, the amount of particles which can be treated can be computed:

$$Nr_{\text{particles}} = \frac{Nr_{\text{molecules}}}{Nr_{\text{atoms per particle}}} = \frac{9.088\cdot 10^{21}}{42.5\cdot 10^{9}} = 2.1375\cdot 10^{11}\text{particles} \tag{B.4}$$

---

[3] https://www.gelest.com/product/SIC2456.3/

[4] https://www.abcr.de/shop/de/11-Cyanoundecyltrichlorosilane-95-77059.html/

[5] https://onlinelibrary.wiley.com/doi/epdf/10.1002/anie.201107097

The volume of one particle is:

$$V_{\text{sphere}} = \frac{4}{3}\pi R_s^3 = \frac{4}{3}\pi 20 \cdot 10^{-3^3} = 3.35 \cdot 10^{-5}\text{mm}^3 = 3.35 \cdot 10^{-8}\text{cm}^3 \tag{B.5}$$

With the assumption 60% of the total volume is occupied with particles, give the following volume of particles which can be treated:

$$V_{\text{Treated particles}} = Nr_{\text{particles}}\frac{V_{\text{sphere}}}{60\%} = 2.13 \cdot 10^{11}\frac{3.35 \cdot 10^{-8}}{0.6} = 11.9 \cdot 10^3\text{cm}^3 = 11.9\text{l} \tag{B.6}$$

C Force - Displacement graph clear glass 4mm

Measurement data:

Brand:	Sili beads
Type:	M
Diameter:	4mm
Young modules:	65GPa
Poisson's ratio:	0.17
Date:	18 June 2019
Humidity:	55.7±0.8%
Temperature:	22.4±0.2°C
Measurement time:	10s
Note(s):	The displacement was moved artificially to zero when the force starts to increases. This was done by, calculating a polynomial of the first order over the loading points where the normal force is greater as 5mN. To avoid the data cannot be read, after 10 measurements the displacement is moved artificially by adding 10μm.

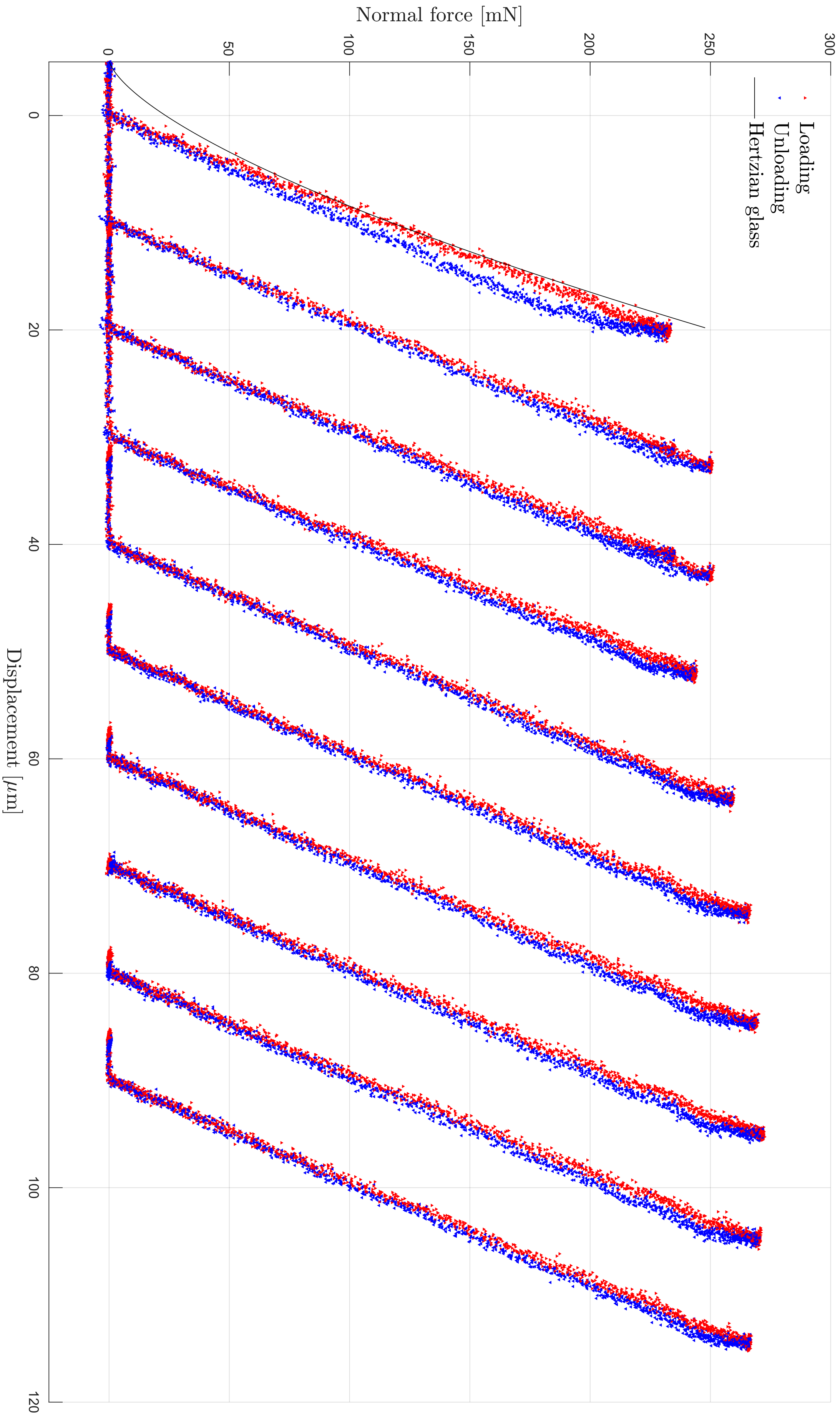
Normal force [mN]
0
50
100
150
200
250
300
Displacement [μm]
0
20
40
60
80
100
120
Loading
Unloading
Hertzian glass

D Force - Displacement graph treated glass 4mm

Measurement data:

Brand:	Mühlmeier
Type:	Diamond pearls
Diameter:	4mm
Young modules:	85GPa
Poisson's ratio:	0.17
Date:	15 May 2019
Humidity:	43.7±0.8%
Temperature:	22.0±0.2°C
Measurement time:	10s
Note(s):	The displacement was moved artificially to zero when the force starts to increases. This was done by, calculating a polynomial of the first order over the loading points where the normal force is greater as 5mN. To avoid the data cannot be read, after 10 measurements the displacement is moved artificially by adding 10μm.

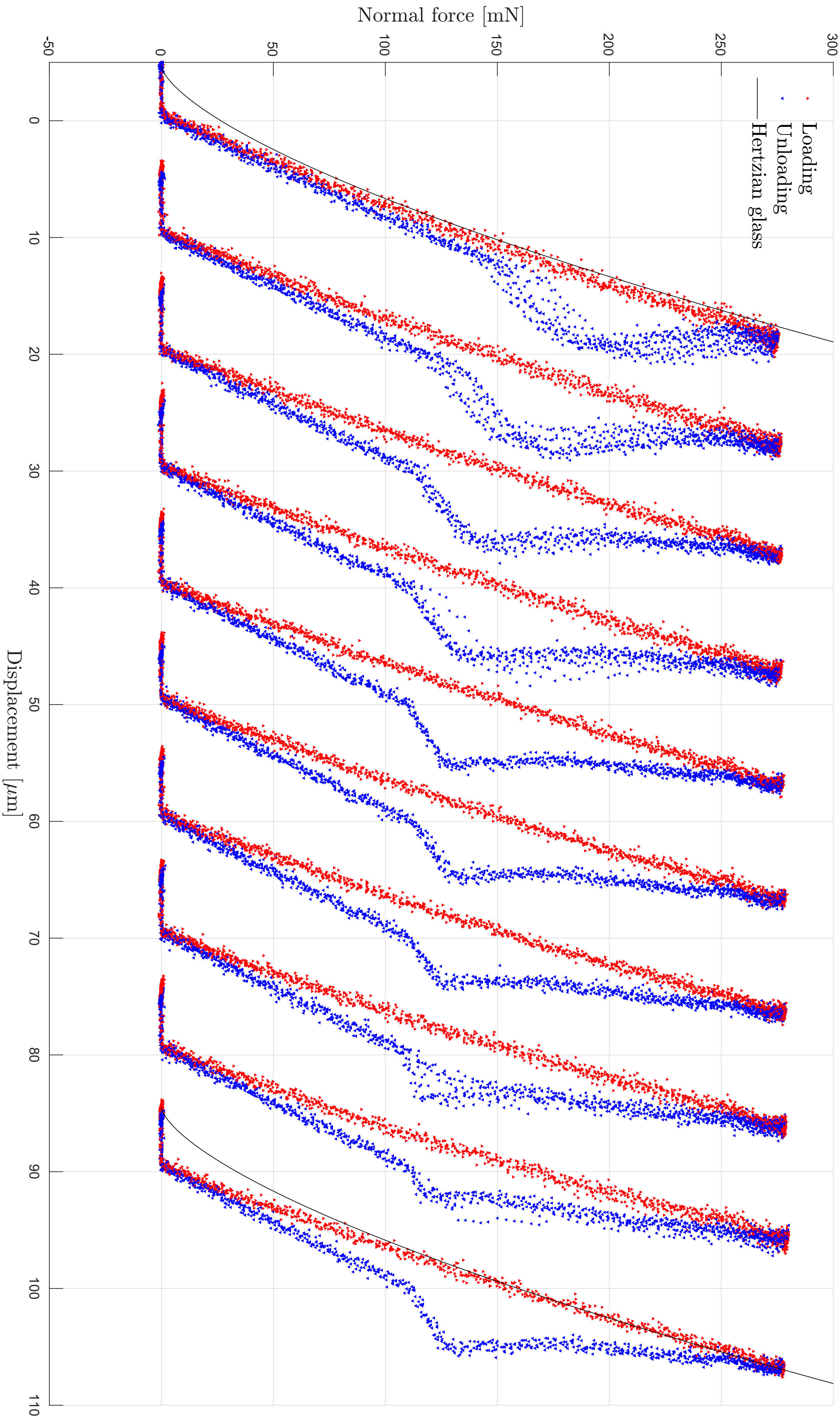
Normal force [mN]
-50
0
50
100
150
200
250
300
Displacement [μm]
0
10
20
30
40
50
60
70
80
90
100
110
Loading
Unloading
Hertzian glass

E Force - Displacement graph treated glass 6mm

Measurement data:

Brand:	Sili beads
Type:	M
Diameter:	6mm
Young modules:	65GPa
Poisson's ratio:	0.17
Date:	13 May 2019
Humidity:	41.1±0.9%
Temperature:	22.8±0.2°C
Measurement time:	10s
Note(s):	The displacement was moved artificially to zero when the force starts to increases. This was done by, calculating a polynomial of the first order over the loading points where the normal force is greater as 5mN. To avoid the data cannot be read, after 10 measurements the displacement is moved artificially by adding 10μm.

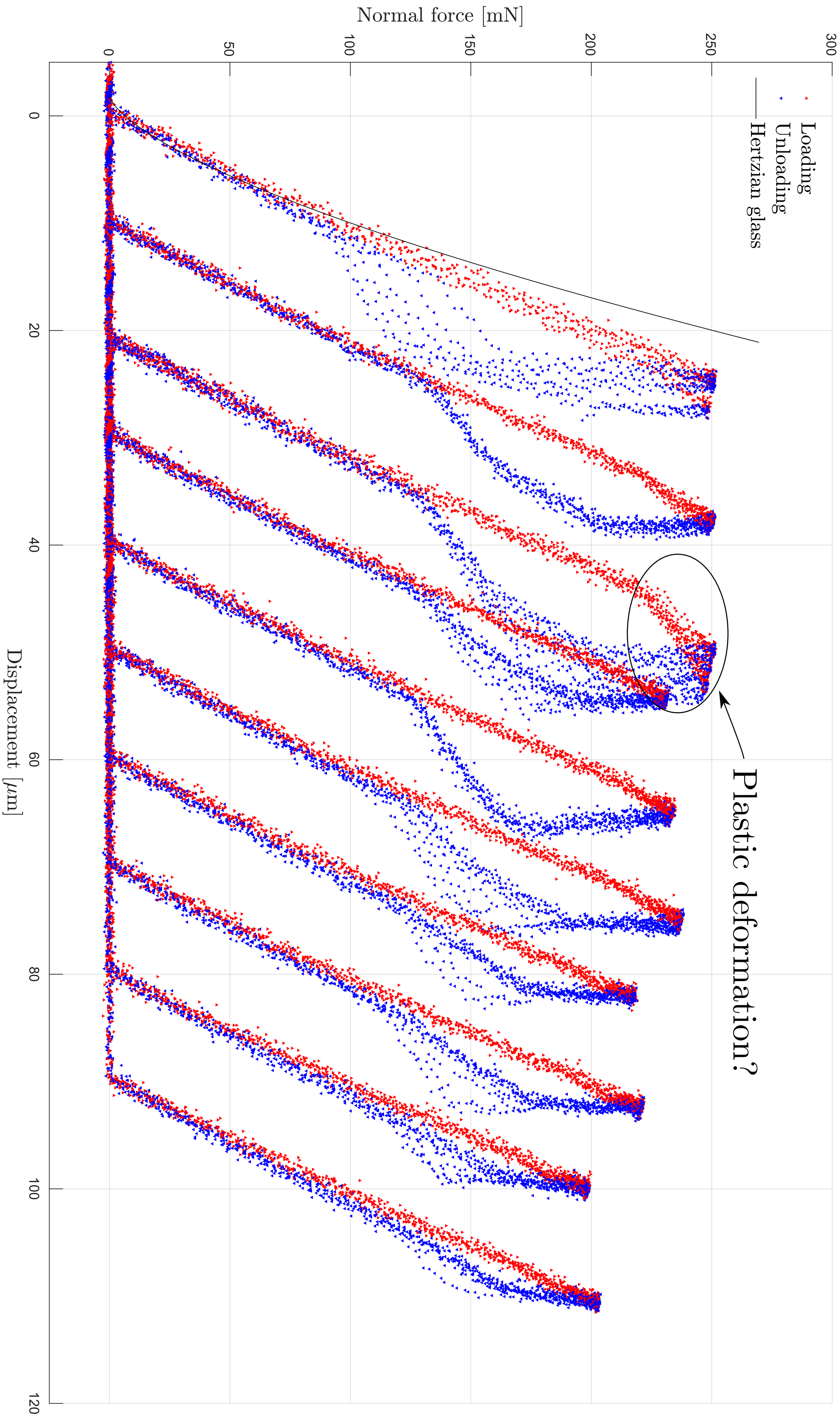
Normal force [mN]
0
50
100
150
200
250
300
Displacement [μm]
0
20
40
60
80
100
120
Loading
Unloading
Hertzian glass
Plastic deformation?

F Force - Displacement graph high polymerized spot

Measurement data:

Brand:	Sili beads
Type:	M
Diameter:	6mm
Young modules:	65GPa
Poisson's ratio:	0.17
Date:	10 May 2019
Humidity:	43.8±1.2%
Temperature:	23.7±0.3°C
Measurement time:	10s
Note(s):	The displacement was moved artificially to zero when the force starts to increases. This was done by, calculating a polynomial of the first order over the loading points where the normal force is greater as 5mN.

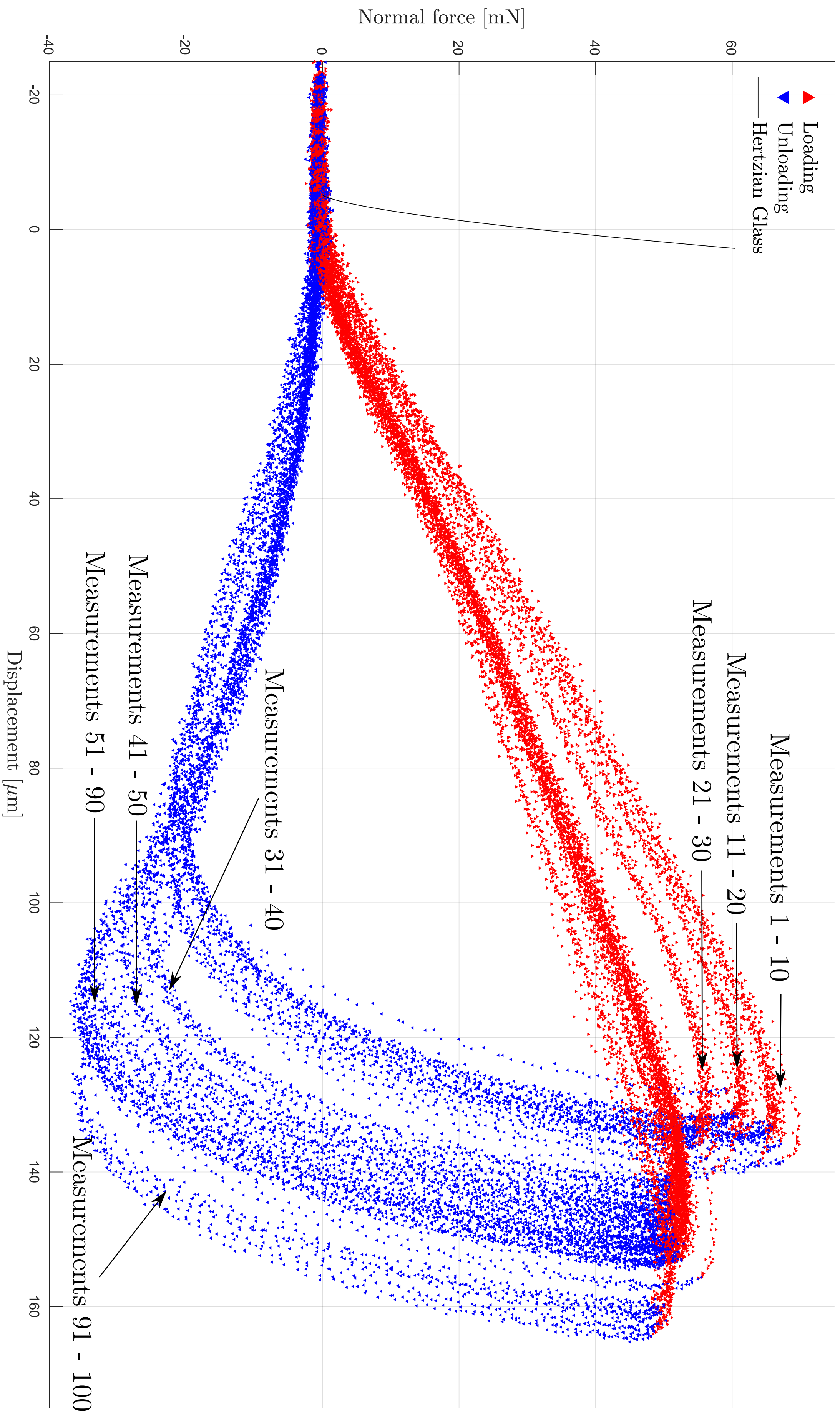
Normal force [mN]
-40
-20
0
20
40
60
Displacement [μm]
-20
0
20
40
60
80
100
120
140
160
Loading
Unloading
Hertzian Glass
Measurements 1 - 10
Measurements 11 - 20
Measurements 21 - 30
Measurements 31 - 40
Measurements 41 - 50
Measurements 51 - 90
Measurements 91 - 100

G Force - Displacement graph increasing normal force

Measurement data:

Brand:	Sili beads
Type:	M
Diameter:	6mm
Young modules:	65GPa
Poisson's ratio:	0.17
Date:	20 June 2019
Humidity:	63.9±0.9%
Temperature:	21.3±0.2°C
Measurement time:	60s
Note(s):	The responses were artificial moved such that, a continues graph was obtained. This was done by; first calculating a polynomial of order one over the loading point where a force was higher as 5mN and, second when the discontinuity starts, the bending point was used as a fix point. There were two discontinuities in the loading curve.

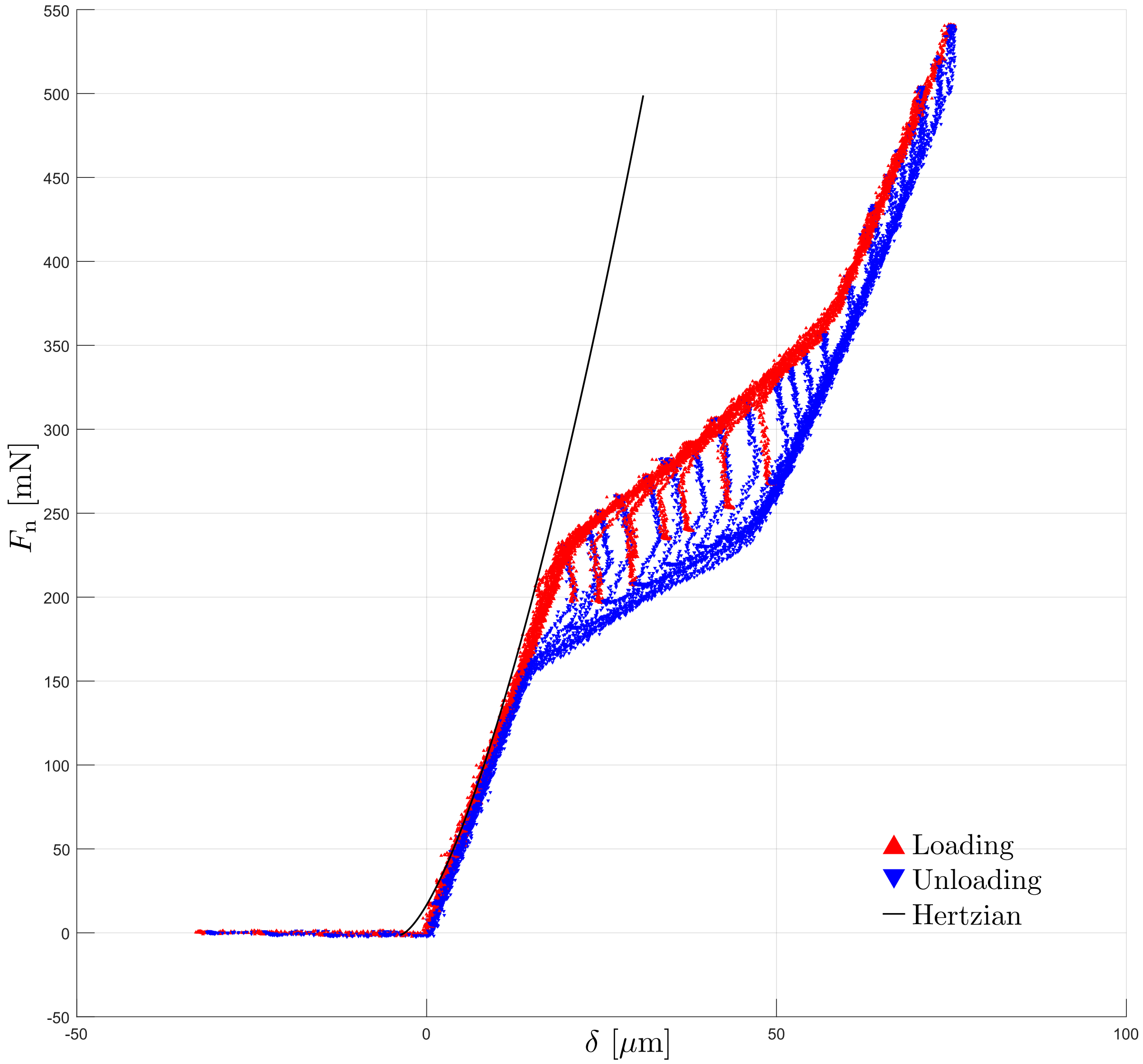
550
500
450
400
350
300
250
200
150
100
50
0
-50
F_n [mN]
-50
0
50
100
δ [μm]
▲ Loading
▼ Unloading
— Hertzian